The Plant Cell, Vol. 24: 4819–4836, December 2012, www.plantcell.org

Evolution from the Prokaryotic to the Higher Plant Chloroplast Signal Recognition Particle: The Signal Recognition Particle RNA Is Conserved in Plastids of a Wide Range of Photosynthetic Organisms[W]

Chantal Träger,[a,1] Magnus Alm Rosenblad,[b,1] Dominik Ziehe,[a] Christel Garcia-Petit,[c] Lukas Schrader,[a] Klaus Kock,[d] Christine Vera Richter,[a] Birgit Klinkert,[e] Franz Narberhaus,[e] Christian Herrmann,[d] Eckhard Hofmann,[f] Henrik Aronsson,[c] and Danja Schünemann[a,2]

[a] Molecular Biology of Plant Organelles, Ruhr-University Bochum, 44780 Bochum, Germany
[b] Department of Chemistry and Molecular Biology, University of Gothenburg, SE-405 30 Gothenburg, Sweden
[c] Department of Biological and Environmental Sciences, University of Gothenburg, SE-405 30 Gothenburg, Sweden
[d] Physical Chemistry I, Ruhr-University Bochum, 44780 Bochum, Germany
[e] Microbial Biology, Ruhr-University Bochum, 44780 Bochum, Germany
[f] Protein Crystallography, Ruhr-University Bochum, 44780 Bochum, Germany

The protein targeting signal recognition particle (SRP) pathway in chloroplasts of higher plants has undergone dramatic evolutionary changes. It disposed of its RNA, which is an essential SRP component in bacteria, and uses a unique chloroplast-specific protein cpSRP43. Nevertheless, homologs of the conserved SRP54 and the SRP receptor, FtsY, are present in higher plant chloroplasts. In this study, we analyzed the phylogenetic distribution of SRP components in photosynthetic organisms to elucidate the evolution of the SRP system. We identified conserved plastid SRP RNAs within all nonspermatophyte land plant lineages and in all chlorophyte branches. Furthermore, we show the simultaneous presence of cpSRP43 in these organisms. The function of this novel SRP system was biochemically and structurally characterized in the moss *Physcomitrella patens*. We show that *P. patens* chloroplast SRP (cpSRP) RNA binds cpSRP54 but has lost the ability to significantly stimulate the GTPase cycle of SRP54 and FtsY. Furthermore, the crystal structure at 1.8-Å resolution and the nucleotide specificity of *P. patens* cpFtsY was determined and compared with bacterial FtsY and higher plant chloroplast FtsY. Our data lead to the view that the *P. patens* cpSRP system occupies an intermediate position in the evolution from bacterial-type SRP to higher plant-type cpSRP system.

INTRODUCTION

Only three ribonucleoprotein particles are universally conserved in all domains of life: the ribosome, RNase P, and the signal recognition particle (SRP). Cytosolic SRP plays a critical role in cotranslational targeting of proteins to the plasma membrane of prokaryotes and the endoplasmic reticulum of eukaryotes (Grudnik et al., 2009; Saraogi and Shan, 2011). In bacteria, SRP binds the signal sequence of a newly synthesized protein emerging out of the ribosomal exit tunnel (Luirink et al., 1992; Halic et al., 2006). By interaction with the SRP receptor FtsY (Luirink et al., 1994), the ribosome-nascent-chain complex is guided to the SecYEG protein-conducting channel in the plasma membrane (Valent et al., 1998). SRP consists of a protein component, Ffh (homolog of eukaryotic SRP54), and an SRP RNA (Poritz et al., 1990). Both the receptor protein FtsY and Ffh are SIMIBI (for signal recognition particle, MinD, and BioD) class GTPases composed of highly conserved N- and G-domains, which interact upon complex formation in a GTP-dependent pseudohomodimerization and activate each other's GTPase activity (Freymann et al., 1997; Montoya et al., 1997; Powers and Walter, 1997; Focia et al., 2004). In Ffh, a C-terminal M-domain facilitates SRP RNA binding and signal sequence recognition (Zopf et al., 1990; Batey et al., 2000). The highly conserved SRP RNA is crucial for *Escherichia coli* cell viability (Ribes et al., 1990) and has two essential functions as it accelerates the formation of the Ffh-FtsY complex at least 200-fold and stimulates its GTPase activity (Peluso et al., 2000, 2001; Siu et al., 2007; Zhang et al., 2008). Since chloroplasts originate from cyanobacteria, the finding of a bacterial-type chloroplast SRP (cpSRP) in higher plants was unsurprising. However, two observations clearly distinguished the cpSRP pathway from the bacterial SRP: (1) Two different SRPs were identified, one for the posttranslational transport of the nuclear-encoded light-harvesting chlorophyll *a*/*b* binding proteins (LHCPs) to the thylakoid membrane, consisting of the Ffh homolog cpSRP54 and the unique protein cpSRP43, plus one for the cotranslational transport of at least some plastid-encoded proteins consisting of cpSRP54

[1] These authors contributed equally to this work.
[2] Address correspondence to danja.schuenemann@rub.de.
The authors responsible for distribution of materials integral to the findings presented in this article in accordance with the policy described in the Instructions for Authors (www.plantcell.org) are: Magnus Alm Rosenblad (magnus.almrosenblad@cmb.gu.se) and Danja Schünemann (danja.schuenemann@rub.de).
[W] Online version contains Web-only data.
www.plantcell.org/cgi/doi/10.1105/tpc.112.102996

only; (2) both the post- and cotranslational transport works in the absence of the universally conserved SRP RNA (Franklin and Hoffman, 1993; Schuenemann et al., 1998; Amin et al., 1999; Klimyuk et al., 1999; Nilsson et al., 1999; Hutin et al., 2002; Richter et al., 2010). The cpSRP43 is composed of an ankyrin repeat domain and three chromo domains, and in the posttranslational SRP pathway, it binds to a positively charged motif in the C-terminal tail of cpSRP54 to form a stable heterodimer in the stroma (Funke et al., 2005; Holdermann et al., 2012). This heterodimer binds its hydrophobic cargo protein, LHCP, to form the soluble transit complex (Schuenemann et al., 1998). With the participation of the membrane-bound GTPase, cpFtsY, this complex is targeted to the Alb3 translocase in the thylakoid membrane (Moore et al., 2000, 2003; Bals et al., 2010; Falk et al., 2010; Lewis et al., 2010; Dünschede et al., 2011).

The finding that no SRP RNA is needed to facilitate SRP-dependent protein transport in chloroplasts raised the question of how the cpSRP system can bypass the requirement for an SRP RNA. Interestingly, kinetic analyses have shown that the cpSRP GTPases (cpSRP54 and cpFtsY) are as efficient in complex formation as their bacterial homologs in presence of an SRP RNA (Jaru-Ampornpan et al., 2007, 2009). The analysis of the crystal structure of *Arabidopsis thaliana* cpFtsY (Stengel et al., 2007; Chandrasekar et al., 2008) indicates that in contrast with its prokaryotic homolog, it has a preorganized conformation more conducive for interaction with cpSRP54. This closed conformation bypasses some structural rearrangements that limit the rate of complex formation between the bacterial SRP GTPases (Chandrasekar et al., 2008). Furthermore, the closed conformation of cpFtsY effects the position of an Asp residue, which is located within the highly conserved TKLD sequence of the GIV motif. This motif belongs to five highly conserved motifs (GI to GV) in the G-domain involved in nucleotide binding and hydrolysis. In *Arabidopsis* cpFtsY, the Asp is shifted toward the guanine base of GTP, which is supposed to lead to an optimized coordination of GTP within the nucleotide binding pocket (Chandrasekar et al., 2008). In the open structure of bacterial FtsY, the analogous Asp (Asp-449 in *E. coli* or Asp-356 in *Thermus aquaticus*) is withdrawn and its contribution to GTP recognition is minor (Montoya et al., 1997; Shan and Walter, 2003; Jaru-Ampornpan et al., 2007; Reyes et al., 2007). It was suggested that this modified position of the Asp residue in cpFtsY contributes to the significantly higher nucleotide specificity compared with prokaryotic FtsY (Jaru-Ampornpan et al., 2007; Chandrasekar et al., 2008). Besides the closed conformation of cpFtsY, the M-domain of cpSRP54 was shown to play an important role for an efficient interaction between the cpSRP GTPases by stimulating complex formation (Jaru-Ampornpan et al., 2009).

So far, molecular studies of SRP-dependent protein transport in chloroplasts have been performed exclusively in higher plants. However, bioinformatic studies predicted the presence of plastid SRP RNA genes on the plastome of some organisms of the red lineage and of some basal green algae (Packer and Howe, 1998; Rosenblad and Samuelsson, 2004; Richter et al., 2008). As no cpSRP43 homologs have been identified in these organisms, it was assumed that these organisms might contain the classic prokaryotic SRP in their plastids. Furthermore, current data support the view that the cpSRP43 replaced the ancestral SRP RNA in the green lineage to enable an efficient transport of LHC proteins.

In this study, we analyzed all available plastid genomes to resolve the phylogenetic distribution of the plastid-encoded SRP RNAs. In addition, we examined the phylogenetic distribution of cpSRP54 and cpSRP43. We show the widespread simultaneous occurrence of a cpSRP RNA and cpSRP43 in chloroplasts of green algae and land plants that evolved earlier than spermatophytes. Molecular details of this novel SRP system were analyzed both on the RNA and protein level using the moss *Physcomitrella patens* as a model.

RESULTS

The Phylogenetic Distribution of Plastid SRP RNA

A comprehensive inventory of SRP components in chloroplasts was performed using all organisms with a sequenced plastid genome as well as partial plastid sequences. For the plastid protein components SRP54 and SRP43, we searched the protein, EST, and SRA databases at the National Center for Biotechnology Information (NCBI) as well as the data made available by different ongoing genome projects, for instance at the Joint Genome Institute.

To analyze the phylogenetic distribution of plastid SRP RNA, we examined 32 organisms of the green algae branch (chlorophytes and secondary plastid-containing algae) and identified plastid-encoded SRP RNAs in all classes (Figure 1; see Supplemental Table 1 online and Supplemental Figure 1 online). Remarkably, among the chlorophytes, only the chlorophyceae contained species (e.g., *Chlamydomonas reinhardtii*) without an identified cpSRP RNA and among the secondary plastid-containing algae *Bigelowiella* encoded a cpSRP RNA, whereas the euglenoid plastids did not. To test whether plastomes of organisms belonging to the streptophytes might also encode cpSRP RNAs, 54 members of the streptophyte lineage (including five seed plants) were analyzed. As expected, no cpSRP RNA gene could be identified in seed plants (spermatophytes). Surprisingly, however, cpSRP RNA genes were found in charophytes (*Chlorokybus* plus five other species) and the land plant branches bryophytes (*Physcomitrella* plus 14 other species), lycophytes (*Huperzia* and *Isoetes*), and even monilophytes (*Pteridium* plus 27 other species) (Figure 1; see Supplemental Table 1 online). In fact, only one genus, *Selaginella*, belonging to the lycophytes, was identified that encoded no cpSRP RNA on its plastome. Therefore, our data modify published analyses (e.g., Rosenblad and Samuelsson, 2004) and show that the presence of a plastid-encoded SRP RNA is almost ubiquitous within the streptophytes with the exception of spermatophytes and some lycophytes.

Previously, it has been reported that SRP RNA genes have been identified on the primary plastid genomes of red algae, on secondary plastid genomes of heterokontophytes and a cryptophyte (Packer and Howe, 1998; Rosenblad and Samuelsson, 2004). This finding, together with the identification of plastid SRP54 and the absence of cpSRP43 homologs, led to the assumption that all organisms of the red lineage might contain the classical bacterial-type SRP (Rosenblad and Samuelsson, 2004). Contrary to this expectation, the extended analysis

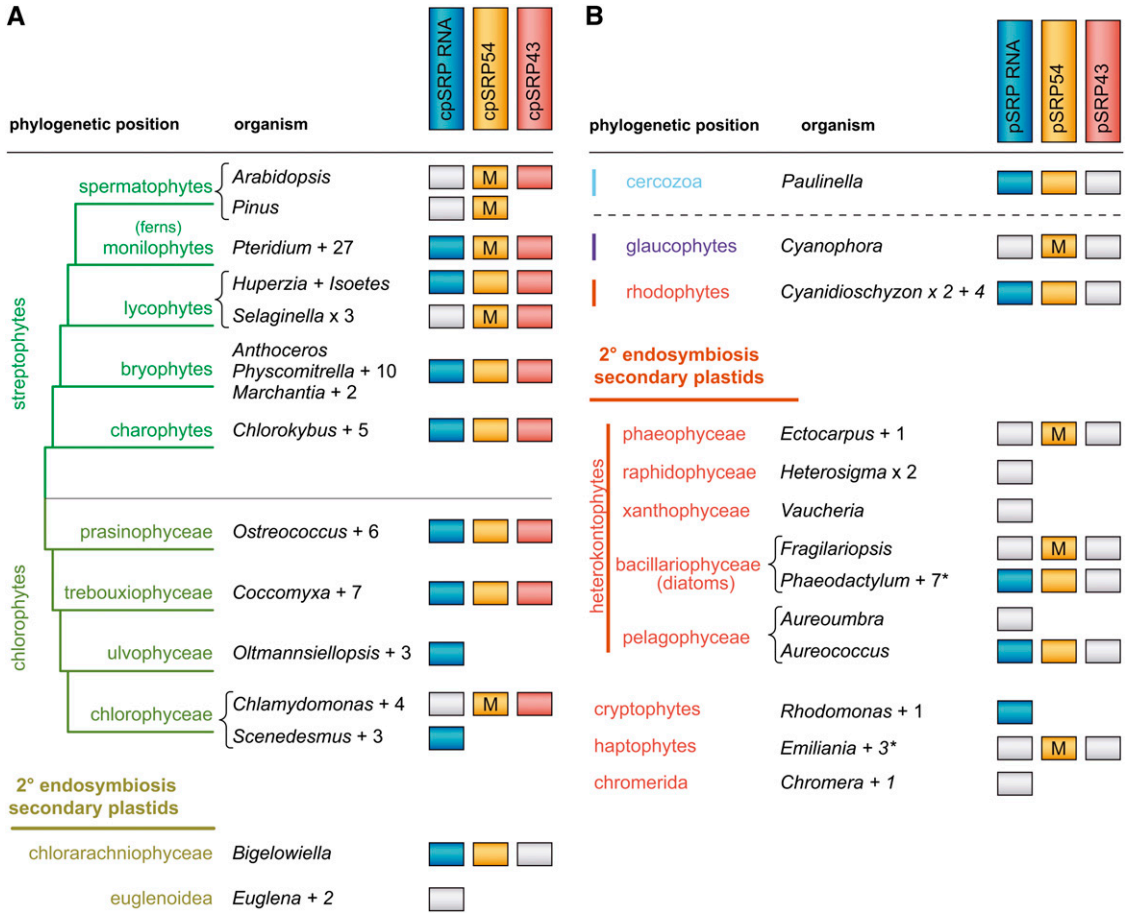

Figure 1. Phylogenetic Distribution of Plastid SRP RNA, Plastid SRP54, and SRP43.

Streptophytes, chlorophytes, and secondary plastid–containing green algae **(A)**; red lineage and others **(B)**. Organisms with a secondary plastid of red algal origin are listed together with the glaucophyte branch and *Paulinella*, which has a plastid acquired from a recent parallel endosymbiosis event and is separated by a dashed line. Analyzed phylogenetic branches are shown with the organisms with the most identified plastid SRP components acting as representatives. *Arabidopsis* and *Pinus* in the spermatophytes serve as model organisms for the angiosperms and gymnosperms, respectively. Numbers after organism names refer to the number of additional species in which a plastid SRP RNA has or has not been identified. Colored boxes refer to found components, white boxes refer to missing components, and in cases no boxes are shown no sequences were available for analysis. "M" refers to mutations in the RNA binding motif of plastid SRP54. Asterisks indicate two added tertiary plastids of diatom origin and one added tertiary plastid of haptophyte origin from dinoflagellate species that are included in the bacillariophyceae or the haptophytes, respectively.

including 30 members of the red branch showed several groups in which the plastid SRP RNA has been lost (Figure 1; see Supplemental Table 1 online). All plastids from rhodophytes (five species) encoded a plastid SRP RNA, but the secondary plastid-containing organisms from eight different phylogenetic-branches showed a much more patchy distribution of the gene. For instance, the diatom and pelagophyte plastome from *Fragilariopsis* and *Aureoumbra*, respectively, lack the gene. Furthermore, no plastid SRP RNA could be found in the other branches of heterokont algae (phaeophyceae, raphidophyceae, and xanthophyceae), in the chromerida, and in the analyzed haptophytes (e.g., *Emiliania*), including the *Karlodinium* tertiary plastid of haptophyte origin (Figure 1; see Supplemental Table 1 online).

In addition to members of the green and red lineage, *Cyanophora* as the only organism from the glaucophyte branch with a sequenced plastid genome and *Paulinella* belonging to the cercozoa were analyzed. We could not identify a plausible plastid SRP RNA candidate in *Cyanophora* despite allowing for many mutations and comparing the genome sequence to other plastid SRP RNA coding regions. Unsurprisingly, however, the large 1-megabase plastid genome of the endosymbiont in *Paulinella* encoded a plastid SRP RNA with high similarity to cyanobacterial homologs, consistent with the fact that the endosymbiontic event occurred quite recently.

Overall, we show that the SRP RNA is conserved in plastids of a wide range of photosynthetic organisms. Here, the most surprising result is the identification of chloroplast-encoded SRP RNAs within all nonspermatophyte land plant lineages. However, some phylogenetic branches contain organisms with no plastid SRP RNA genes, indicating that the loss of the plastid SRP RNA has occurred several times during evolution, both in red and green plastid lineages.

Genomic Location and Promoter Analysis of the Plastid SRP RNAs

Most of the predicted plastid SRP RNAs were found within highly conserved gene clusters (Figure 2; see Supplemental Figure 2 online). Within the streptophytes, all cpSRP RNAs (except the one in *Chaetosphaeridium*; see Supplemental Figure 2 online) were located downstream of *petN* in the conserved *petN-trnC* region. In most cases, this region is part of the conserved *petN-trnC-rpoB-rpoC1-rpoC2* cluster, although the cluster has been split in the bryophyte *P. patens* and several monilophytes. In *P. patens*, the *petN-trnC* region is clustered with pet genes due to an inversion of a large part of the plastome (Sugiura et al., 2003). Such inversions leading to structural rearrangements of the gene order have also been described for plastid genomes of monilophytes (Gao et al., 2011).

Consistent with cpSRP RNA gene location in streptophytes, the cpSRP RNAs in chlorophytes and the secondary plastid–containing green algae *Bigelowiella* are also mostly encoded upstream of the *trnC-rpoB-rpoC1-rpoC2* gene cluster. However, the cpSRP RNA gene in species from the ulvophyceae (e.g., *Oltmannsiellopsis*) and chlorophyceae (e.g., *Scenedesmus*) shows a different localization (Figure 2; see Supplemental Figure 2 online), which reflects the overall more variable plastid gene order in chlorophytes (Letsch and Lewis, 2012).

In the red branch, the plastid SRP RNA is found upstream of *psbX*, except in *Aureococcus* (Figure 2) and *Thalassiosira* (see Supplemental Figure 2 online). In *Thalassiosira pseudonana*, the region contains a large insertion so that the gene is located close to *dnaB-trnF*, which otherwise are upstream of *psbX*, and in *Thalassiosira oceanica* this is further split.

The location of the plastid SRP RNA gene in plastid genomes from both the red and green groups is thus surprisingly conserved. Conserved TATA-box promoters, typically TATAAT, were found upstream of the predicted sequences at a distance of 4 to 10 nucleotides (Figure 3; see Supplemental Figure 3 online).

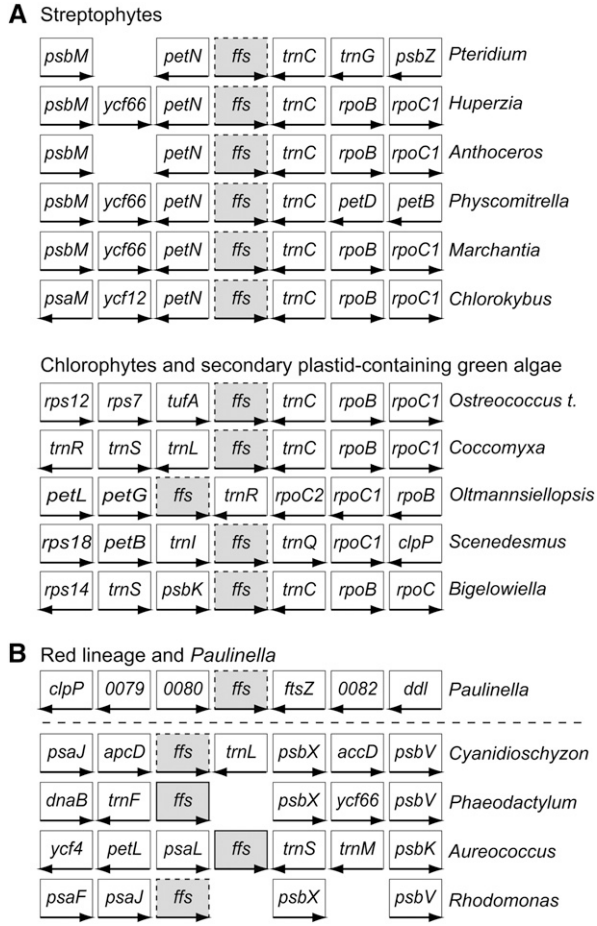

Figure 2. Gene Order for Selected Plastid SRP RNA Regions.

Gene order in the plastid SRP RNA (*ffs*) region for the organisms of Figure 1 with streptophytes, chlorophytes, and secondary plastid–containing green algae **(A)** and red lineage and *Paulinella* **(B)**. Arrows show the direction of each gene. Directions were changed from the annotation to align conserved regions and plastid SRP RNA. Dashed line of the *ffs* box refers to predicted plastid SRP RNAs; full line refers to the *ffs* being annotated. Numbers indicate unnamed *Paulinella* genes.

Verification of Plastid-Encoded SRP RNA Expression

To verify the expression of predicted plastid SRP RNAs, we selected seven organisms representing different phylogenetic branches: the monilophyte *Psilotum nudum*, the moss *P. patens,* the liverwort *Marchantia polymorpha*, the red alga *Porphyra purpurea*, the diatom *T. pseudonana*, the pelagophyte *Aureococcus anophagefferens*, and the cryptophyte *Rhodomonas salina*. All plastid SRP RNAs from the chosen species are expressed as verified by RT-PCR (see Supplemental Figure 4 online) and subsequent sequencing (see Supplemental Methods 1 online).

In GenBank, we identified an RNA sequence from the chlorophyte *Codium fragile*, which was annotated as a highly abundant ribosomal 4.5 S RNA (Francis et al., 1987), although the authors noticed a small similarity to the 4.5 S SRP RNA of *E. coli*. Notably, our analysis revealed that the plastid-encoded *Codium* RNA is misannotated because it is similar to the cpSRP RNAs of the green algae *Oltmannsiellopsis* and *Bryopsis* from the same phylogenetic group but not to any chlorophyte rRNAs (see Supplemental Figure 1 online; data not shown). Therefore, the described *Codium* RNA can serve as additional evidence for the expression of green algal cpSRP RNAs.

Plastid SRP RNA Sequences and Structures

Due to the cyanobacterial origin of the plastid SRP RNA, we expected similarities between the plastid RNAs and the SRP RNA found in most eubacteria. This molecule is characterized by a conserved domain made up of one asymmetrical, one symmetrical, and an apical loop joined together with helices (Rosenblad et al., 2009). The highly conserved apical loop of the SRP RNA in eubacteria is generally a GNRA or URRC tetra loop (N: A, C, G, or U; R: A or G), but a few exceptions seem to exist in which the loop is composed of URRU or five nucleotides (Rosenblad et al., 2009). Another conserved feature of SRP RNAs is the presence of three universally conserved nucleotides (G, A, and C) in the symmetrical

A Streptophytes

-10 box	spacer	*ffs*	organism
TGC TATACT	TGATC	GGGATTGT...	*Pteridium*
AAT TATCCT	TAATGTA	GGGTTGTC...	*Huperzia*
TAT TACCAT	TAATACA	GGGTTGTT...	*Anthoceros*
ATT TATTCT	TAATGTTA	GGATTATC...	*Physcomitrella*
TTT TAATCT	TATGAT	GGGTTGTC...	*Marchantia*
TGT TAAAAT	AGTAAGCATA	ACCCTCAA...	*Chlorokybus*

Chlorophytes and secondary plastid-containing green algae

-10 box	spacer	*ffs*	organism
AAA TATACT	ATTTAGTA	GTCCTACT...	*Ostreococcus t.*
TAT TATACT	TGACAA	GCTCACAA...	*Coccomyxa*
AGG TAAACT	ACTATTAA	GGATTTTA...	*Oltmannsiellopsis*
TGA TATTTT	ATTAAGTAA	GCCCAGAA...	*Scenedesmus*
AAT TATAAT	AAATGT	GTAAACTG...	*Bigelowiella*

B Red lineage and *Paulinella*

-10 box	spacer	*ffs*	organism
TGC TACAAT	GGACAT	GACTCGGA...	*Paulinella*
TGG TATAAT	TTCGTTA	GCCCGCAA...	*Cyanidioschyzon*
GCC TATAAT	AAGCTTTG	GGTATAGT...	*Phaeodactylum*
TGA TACAAT	AATTAT	GTATCTAG...	*Aureococcus*
CTA TATTAT	ATTCTA	ATCCTGGT...	*Rhodomonas*

Figure 3. Promoter Sequences for Selected Organisms with Plastid SRP RNAs.

Examples of TATA promoter regions of plastid SRP RNA (*ffs*) for organisms of Figure 1 with streptophytes, chlorophytes, and secondary green algae **(A)** and red lineage and *Paulinella* **(B)**. Depicted are the −10 box (TATA consensus region), the spacer, and the beginning of *ffs*. This structure is also present in previously analyzed SRP RNA promoters (Rosenblad and Samuelsson, 2004).

loop, which must be present at their exact locations for the SRP RNA to be functional. The SRP RNA of the cyanobacterium *Synechococcus* has these typical structural features (Figure 4A). To predict SRP RNA genes, our analyses included primary sequence and secondary structure as well as comparison of predictions from closely related organisms. As the 5′ and 3′ ends of the RNAs are difficult to predict, promoter analysis and identification of putative termination signals were integrated in the analysis. In most cases, the approximate ends of the RNA could be established. An overview of full plastid SRP RNA alignments and secondary structure examples is given in Supplemental Figure 1 online.

With only one exception, all plastid SRP RNAs from the red lineage (16 species) showed the bacterial consensus structural elements (Figure 4A; see Supplemental Figure 1 online). Only the plastid SRP RNA of the dinoflagellate *Durinskia*, which harbors a plastid of diatom origin, has an atypical AUAC tetra loop instead of the GNRA tetra loop present in all other organisms of the red lineage.

Likewise, the basal prasinophyceae (seven species) and the trebouxiophyceae (eight species) encoded cpSRP RNAs similar to the usual bacterial consensus elements including the GNRA tetra loops, although a few variations could be seen: an AAAA loop in *Oocystis* and GATA in *Pedinomonas* (Figure 4A; see Supplemental Figure 1 online). However, in the ulvophyceae (four species) and the chlorophyceae (four species), the apical loop displayed more variation, with TTTA, CTGA, and ATAT. In addition, the length of the apical loop varies with five nucleotides CTAAA in *Bryopsis*, six nucleotides TTAATA in *Codium*, or even less than four nucleotides in *Stigeoclonium* and *Schizomeris*. The *Bryopsis* cpSRP RNA also had a mismatch in the base pair closing the loop, a very rare feature in bacterial SRP RNAs (see Supplemental Figure 1 online).

Within the streptophytes, the basal algae *Mesostigma* and *Chlorokybus* have cpSRP RNAs similar to the basal prasinophytes and trebouxiophytes, although with TAAA tetra loops. All other cpSRP RNAs of the streptophyte branches contain the consensus elements that are typical for bacterial SRP RNA, but surprising variations in the apical loop region. While some species contain cpSRP RNAs with apical loops of five nucleotides (e.g., *Huperzia*), seven nucleotides (*Marchantia*), or nine nucleotides (e.g., *Zygnema*), most cpSRP RNAs were predicted to have apical loops expanded to 10 nucleotides (e.g., *Physcomitrella*) (Figure 4A; see Supplemental Figure 1 online).

In conclusion, our data indicate that organisms of the red lineage and basal organisms of the green lineage (prasinophytes, trebouxiophytes, and some charophytes) contain plastid SRP RNAs that are very similar to bacterial SRP RNA, while particularly later evolved organisms in the streptophyte branch contain less conserved plastid SRP RNAs with elongated apical loops. The evolutionary change from the conserved tetra loop structures toward the elongated apical loop structures within the streptophytes is depicted in Figure 4A.

Structure Probing of *P. patens* cpSRP RNA Supports the Predicted Structure

As the predicted structures of plastid SRP RNAs from streptophytes deviate substantially from the canonical bacterial SRP RNA in the size of the apical loop, we intended to verify the structure of the *P. patens* cpSRP RNA experimentally. Therefore, enzymatic probing of radiolabeled in vitro–transcribed cpSRP RNA was performed using increasing concentrations of RNase T1, which cleaves single-stranded RNA after guanine residues (G) (Figure 4B). The prominent RNase T1 cut at G51 in the apical loop even at low enzyme concentrations clearly demonstrates the unpaired conformation of G51 and fully supports the presence of an enlarged apical loop. In addition, T1 probing confirms the predicted unpaired status of the guanine residues in the symmetric and asymmetric loop (G44, G45, and G71) and the predicted paired status of G38 in the stem between these loops supporting the overall structure of the *P. patens* cpSRP RNA (Figure 4B).

Mutations within the SRP RNA Binding Site of Plastid SRP54 Are Phylogenetically Correlated to the Loss of the cpSRP RNA Gene

In a previous study, we demonstrated that cpSRP54 of *Arabidopsis* lacks the ability to bind bacterial SRP RNA due to a mutation of Ser to Val in the SM motif and a mutation of the first Gly to Asp in the GXG motif within the otherwise conserved RNA binding domain (Richter et al., 2008). Furthermore, it was shown that either one of these mutations is sufficient to abolish the SRP RNA binding ability. As this study identified plastid SRP RNAs in

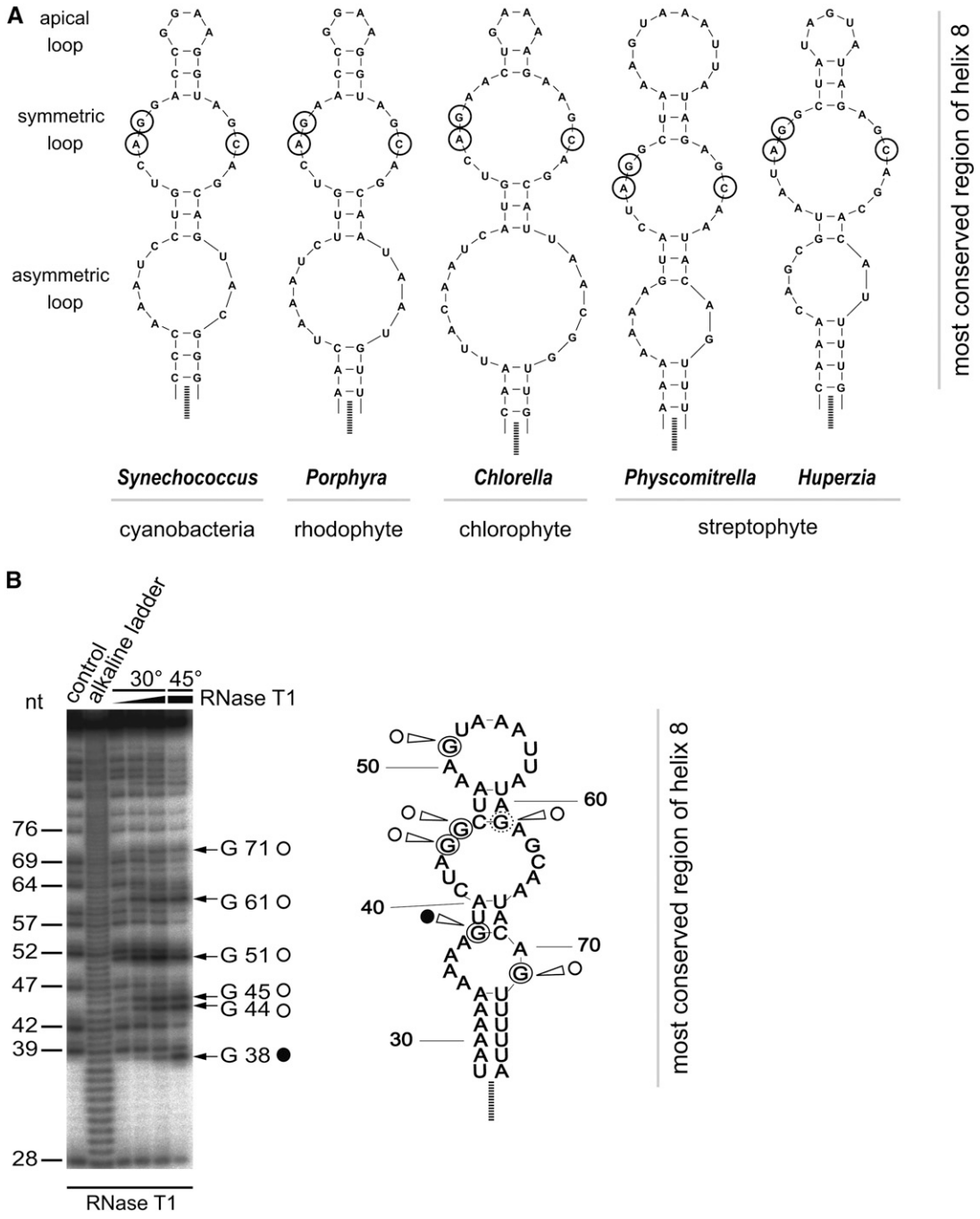

Figure 4. Examples of SRP RNA Structures from Different Phylogenetic Branches and Structure Probing of *P. patens* cpSRP RNA.

(A) The most conserved region of an SRP RNA, usually referred to as helix eight, from the cyanobacterial *Synechococcus* and predicted plastid SRP RNAs from different phylogenetic groups are shown. Loop names are listed beside structures. Universally conserved nucleotides in the symmetric loop are circled.

(B) Structure probing of the *P. patens* cpSRP RNA. Structure probing was done as indicated in Methods with RNase T1 (0.002, 0.005, and 0.01 units at 30°C and 0.01 units at 45°C) and water as control. Closed circles, paired nucleotides; open circles, unpaired nucleotides; nucleotides encircled by a solid or dotted circle have a confirmed position or a position that differs from the predicted structure, respectively. nt, nucleotides

a wide range of photosynthetic organisms, we intended to see if the critical mutations were found only in plastid SRP54 proteins of organisms that lacked a plastid SRP RNA. We analyzed eight plastid SRP54 protein sequences from the red lineage and 28 from the green lineage in addition to plastid SRP54 from *Paulinella* and *Cyanophora* (Figure 5; for a full alignment of plastid SRP54 sequences, see Supplemental Figure 5 online). Indeed, all plastid SRP54 proteins from organisms that did not encode a plastid SRP RNA displayed a mutated SRP RNA binding motif. Furthermore, with just two exceptions (*Pteridium* and *Chaetosphaeridium*), all other organisms that had been found to encode a plastid SRP RNA did not display any of these plastid SRP54 mutations (see Figure 1 for an overview; see Supplemental Table 1 and Supplemental Figure 5 online).

The Phylogenetic Distribution of Plastid SRP43

Identification of plastid SRP43 was made based on the criterion that candidates must display both ankyrin domains and at least one chromo domain. No such protein sequences could be identified in the red branches, glaucophytes, and *Paulinella*, whereas all green plant groups contained reliable candidates (Figure 1). Notably, within the green lineage, the presence of cpSRP43 is not restricted to organisms that lack a cpSRP RNA gene but is also present in those encoding a plastid SRP RNA. These data clearly show that the evolution of cpSRP43 is not correlated to the loss of an SRP RNA. By contrast, the simultaneous presence of cpSRP43 and a cpSRP RNA seems to be the rule within green plants with the exception of *C. reinhardtii* (and some other chlorophyceae), *Selaginella*, and spermatophytes. A summary of the cpSRP43 domain predictions is displayed in Supplemental Figure 6 online, and a full alignment of all cpSRP43s is given in Supplemental Figure 7 online.

In *P. patens*, cpSRP54 Is Able to Bind the cpSRP RNA and cpSRP43

As described above, the cpSRP RNA of streptophytes contains the conserved nucleotides in the symmetric loop that were shown to be important for SRP54 binding but exhibits an unusual structure with regard to the elongated apical loop. To analyze whether cpSRP54 is able to bind this SRP RNA type, the corresponding SRP components of *P. patens* (Pp), cpSRP54, and cpSRP RNA were used in a binding experiment. The SRP components from *E. coli* (Ec) and cpSRP54 from *Arabidopsis* (At) served as positive and negative controls, respectively (Figure 6A). An additional control was performed in absence of RNA. The Pp-cpSRP54 clearly bound the Pp-cpSRP RNA and the Ec-SRP RNA. Notably, an interaction between Ffh from *E. coli* and the Pp-cpSRP RNA was also detected.

In analogy to cpSRP54 of higher plants, the cpSRP54 of *P. patens* harbors the positively charged cpSRP43 binding motif in the C terminus (see Supplemental Figure 5 online). To verify the binding between Pp-cpSRP54 and Pp-cpSRP43, yeast two-hybrid studies were conducted (Figure 6B). The experiment revealed that Pp-cpSRP54 interacts with cpSRP43 of *P. patens* as well as with *Arabidopsis* cpSRP43. As expected, no interaction was observed between Pp-cpSRP43 and Ffh. For these experiments, a cpSRP43 construct was used that corresponded to the longest available cDNA clone (amino acids 185 to 419) but lacked chromo domain one and a small part of ankyrin repeat one. To confirm cpSRP54/cpSRP43 complex formation recombinantly produced cpSRP54 was tested for binding full-length mature cpSRP43 (amino acids 62 to 419) or an N-terminal truncated cpSRP43 construct (amino acids 174 to 419) lacking chromo domain one by gel filtration chromatography. Stable complex formation between cpSRP54 and both cpSRP43 constructs was observed (Figure 6C). Taken together these data

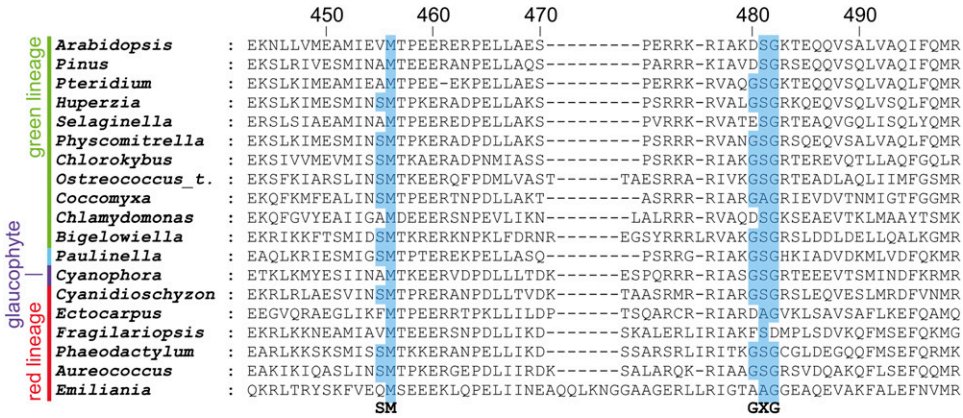

Figure 5. Phylogenetic Distribution of Conserved and Mutated SRP RNA Binding Regions of Plastid SRP54 Sequences.

Alignment of partial plastid SRP54 sequences from the example organisms of Figure 1 containing the conserved or mutated SM···GXG motif (marked in blue). The first amino acid of the SM and GXG motif was shown previously to be critical for SRP RNA binding (Richter et al., 2008). The numbering corresponds to *Arabidopsis* cpSRP54. Organisms without a plastid SRP RNA are from the top: *Arabidopsis*, *Pinus*, *Selaginella*, *Chlamydomonas*, *Cyanophora*, *Ectocarpus*, *Fragilariopsis*, and *Emiliania*.

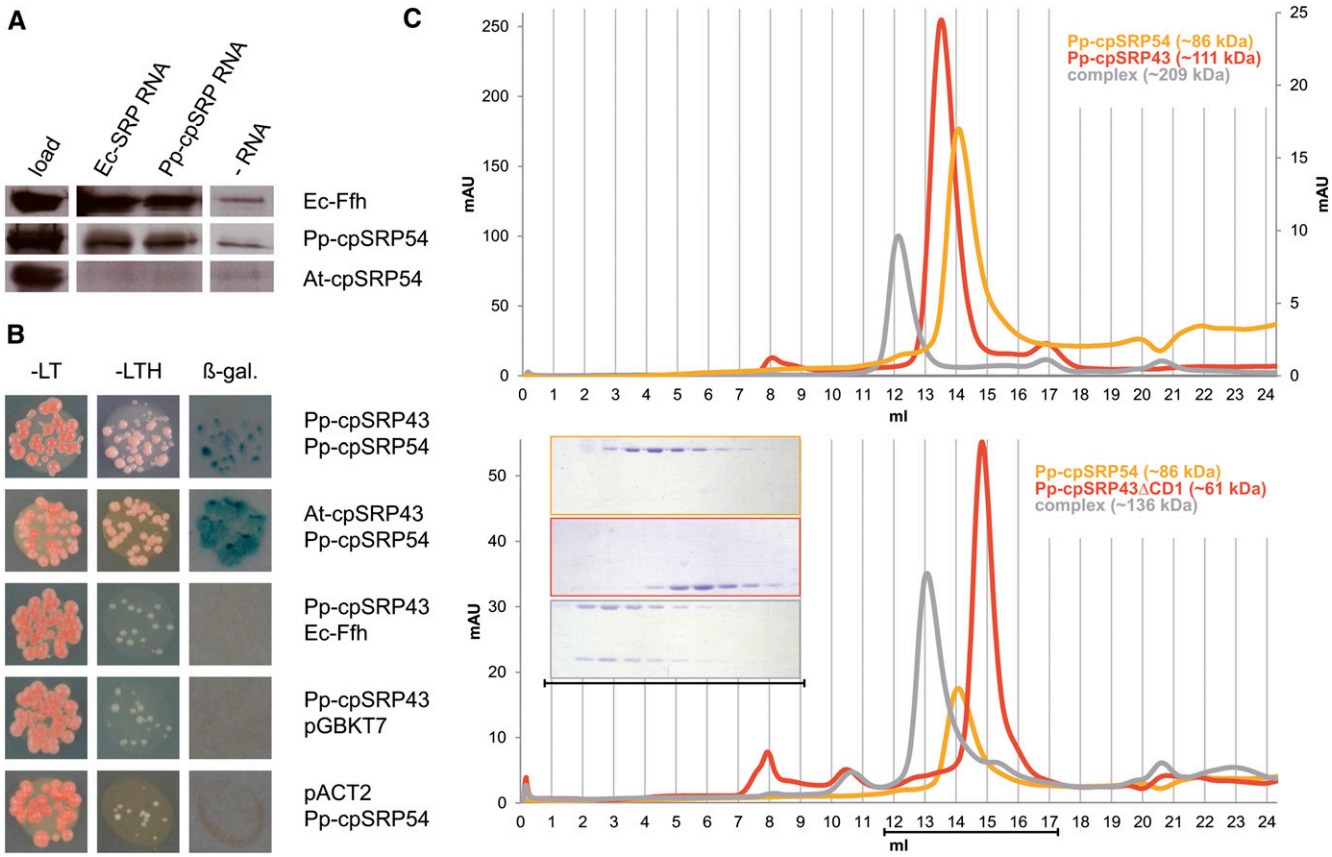

Figure 6. Interaction Studies of *P. patens* cpSRP54 with (cp)SRP RNAs and Different cpSRP43 Proteins.

(A) Radiolabeled in vitro translation products of *E. coli* Ffh and *P. patens* and *Arabidopsis* cpSRP54 (load) were incubated with in vitro–transcribed (cp) SRP RNAs from *E. coli* or *P. patens* or without any RNA (−RNA). RNA bound proteins were separated from unbound ones by anion exchange chromatography as previously described by Richter et al. (2008).

(B) Yeast strain Y190 was cotransformed with pACT2 and pGBKT7 constructs. All cpSRP43 derivatives were cloned into pACT2, whereas the different cpSRP54 and Ffh constructs were cloned into pGBKT7. *P. patens* cpSRP43 used for these studies comprised residues 185 to 419 and lacked the TP, CD1, and a small part of ankyrin repeat one. Cotransformed cells were dotted onto minimal media lacking Leu and Trp (-LT) to check for co-transformation or Leu, Trp, and His (-LTH) to check for interaction. β-Galactosidase (β-gal.) activity of grown colonies was visualized using filter assays.

(C) Analysis of complex formation between Pp-cpSRP54 and full-length mature Pp-cpSRP43 (top panel) and a truncated Pp-cpSRP43 construct (amino acids 174 to 419) (bottom panel). Pp-cpSRP54 (orange line), the Pp-cpSRP43 constructs (red line), or an equimolar mixture of both SRP components (gray line) were analyzed by gel filtration chromatography. Peak fractions were analyzed by SDS-PAGE. As cpSRP54 and full-length mature cpSRP43 showed the same running behavior in SDS-PAGE, Coomassie blue–stained fractions are shown only for the lower chromatography. In the top panel, the *y* axis on the right corresponds to the absorbance (mAU) of cpSRP54.

show that *P. patens* cpSRP54 is able to bind the cpSRP RNA and cpSRP43.

The Ability of *P. patens* cpSRP RNA to Enhance GTP Hydrolysis Is Drastically Reduced

As in the bacterial SRP system, one critical role of the SRP RNA is the stimulation of the GTPase activity of the SRP GTPases Ffh and FtsY when they form a complex, we aimed to characterize the *P. patens* SRP RNA in this regard. Initially, the *P. patens* chloroplast homolog of FtsY was identified. A predicted chloroplast transit sequence (data not shown) and a phylogenetic analysis using chloroplast and cytosolic FtsY sequences clearly point to a chloroplast localization (see Supplemental Figure 8, Supplemental Figure 9, and Supplemental Data Set 1 online). Subsequently, the GTPase activity of recombinant *P. patens* cpSRP54 and cpFtsY and of the corresponding recombinant SRP GTPases of *E. coli* and *Arabidopsis* was measured in the absence and presence of (cp)SRP RNAs from *P. patens* and *E. coli*. In addition, we used the cpSRP RNA from *Ostreococcus*, which has the conserved apical tetra loop and has been shown to bind Pp-cpSRP54 and Ffh previously (Richter et al., 2008). The GTP hydrolysis in presence of the cpSRP GTPases from *P. patens* could be increased twofold by addition of the tetra loop (cp)SRP RNAs of *E. coli* or *Ostreococcus* (Figure 7). The same effect was observed for the *E. coli* SRP GTPases. Interestingly, addition of the cpSRP RNA from *P. patens* harboring the elongated apical loop led to a drastically reduced increase of GTP

hydrolysis using the *P. patens* and the *E. coli* (cp)SRP GTPases (reduction by 80%). As expected, the cpSRP GTPases of *Arabidopsis* were not affected by the addition of any of the tested (cp) SRP RNAs. These data indicate that the *P. patens* SRP RNA might be functionally similar to *E. coli* SRP RNA tetra loop mutants, whose defect is the loss of GTP hydrolysis stimulation of the Ffh-FtsY complex (Spanggord et al., 2005; Siu et al., 2007). As it was shown recently that the SRP RNA distal end is involved in stimulating the GTP hydrolysis in the Ffh-FtsY complex (Ataide et al., 2011), differences in this region of the Pp-cpSRP RNA might also cause its different function. However, it is also possible that the complex formation between the (cp)SRP GTPases is less efficient in presence of Pp-cpSRP RNA compared with tetra loop SRP RNAs as it was shown that mutations within the SRP RNA tetra loop result in slower kinetics to form the Ffh-FtsY complex (Zhang et al., 2008; Shen and Shan, 2010).

The Crystal Structure of *P. patens* cpFtsY Reveals an Overall Closed Conformation and an Unusual P-Loop

To analyze whether *P. patens* cpFtsY is structurally related to the higher plant-type closed or bacterial-type open conformation, the crystal structure was determined at 1.8-Å resolution without bound ligand. A summary of the data collection and refinement statistics is given in Supplemental Table 2 online. We observed two copies within the asymmetric unit, which form a dimer with an interface area of ~1050 Å^2 as determined with the PDBePISA server (Krissinel and Henrick, 2007). There are no indications for biological relevance of this dimer, as the second copy occupies a position different to the location where the highly homologous cpSRP54 would be present in the cpSRP GTPase complex. In our cpFtsY expression construct, the transit peptide (residues 1 to 56) and the membrane targeting site I (residues 57 to 79) have been replaced by a His_6 tag of which the last four residues were included in the model. Residues 220/221 as well as 243 to 246 of the mature protein could not be modeled due to disorder. The overall structure of Pp-cpFtsY displays the typical NG domain structure that characterizes SRP GTPases. The N-domain is composed of a bundle of four α-helices. The G-domain, which is related to the P-loop NTPases, contains all five highly conserved G-motifs (Figures 8A and 9A), which are essential for nucleotide binding and hydrolysis. At the NG interface, the conserved sequence motifs 85-FSGF-88 (conserved only among cpFtsYs of land plants), 120-VLLVSDF-126, 308-LDGTTGL-314, and 340-TARGG-344 are present.

A characteristic feature of the open conformation of bacterial FtsY is a relaxed arrangement of the N-domain helices that becomes more tightly packed in the closed conformation upon complex formation with Ffh. This is especially evident in helix αN2 that needs to undergo a significant rotation for stable FtsY/Ffh complex formation (Egea et al., 2004; Chandrasekar et al., 2008). A conformation very similar to this closed conformation was also observed in the uncomplexed form of *Arabidopsis* cpFtsY (Stengel et al., 2007; Chandrasekar et al., 2008). For the N-domain of our ligand-free *P. patens* cpFtsY structure, we also find a very similar positioning of the N-domain helices, especially of helix αN2 (Figure 8B). Therefore, these data indicate that *P. patens* cpFtsY exhibits an overall closed structure as was shown for *Arabidopsis* cpFtsY.

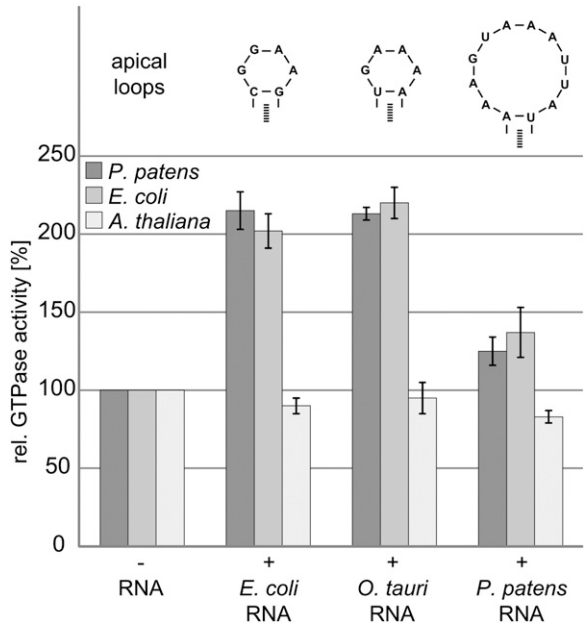

Figure 7. GTP Turnover of SRP GTPases in Absence and Presence of Different (cp)SRP RNAs.

The GTPase activity of recombinant (cp)SRP GTPases [Ffh/cpSRP54 and (cp)FtsY; 200 pmol of each indicated protein] and their activity in the presence of different (cp)SRP RNAs (denoted as RNA) was measured as indicated in Methods. Normalized GTP turnover is given as relative GTPase activity [%], whereby for *E. coli* SRP GTPases 12.7 nmol P_i/h, for *P. patens* cpSRP GTPases 13.3 nmol P_i/h, and for *Arabidopsis* cpSRP GTPases 10.0 nmol P_i/h were set to 100%. The average and SD were calculated from triple determinations and confirmed in at least two independent experiments. Apical loops of the tested (cp)SRP RNAs are depicted on top of each column.

Surprisingly, we find a drastic change in the conformation of the GI motif (P-loop) (Figure 9A). This loop is critical for the coordination of the α- and β-phosphate groups of the substrate NTPs in P-loop NTPases and adopts the canonical GTP binding conformation even in the absence of substrate in all available (cp)FtsY structures except the apo-structure FtsY of *Mycoplasma mycoides* (Gariani et al., 2006; see Discussion). In Pp-cpFtsY, residues of the P-loop form an additional turn of the helix within the GI motif. As this region is remote from crystal contacts, we don't expect the conformation to be imposed by the crystallization conditions. Notably, a superposition of the nucleotide binding pocket of *T. aquaticus* (Ta) FtsY with the Pp-cpFtsY structure indicates that the additional helix turn in the P-loop of Pp-cpFtsY interferes with nucleotide binding as it occupies the binding pocket (Figure 9B). Therefore, our data suggest that a conformational rearrangement of the P-loop is needed to facilitate nucleotide binding in Pp-cpFtsY.

Within the GII motif, which is responsible for the γ-phosphate interaction of the bound nucleotide and the coordination of a magnesium ion, a highly conserved catalytic Arg is present that is important for GTP hydrolysis (Egea et al., 2004; Focia et al., 2004). Within the sequence of Pp-cpFtsY, the Arg (Arg-221) is present but in the structure it is disordered, probably as

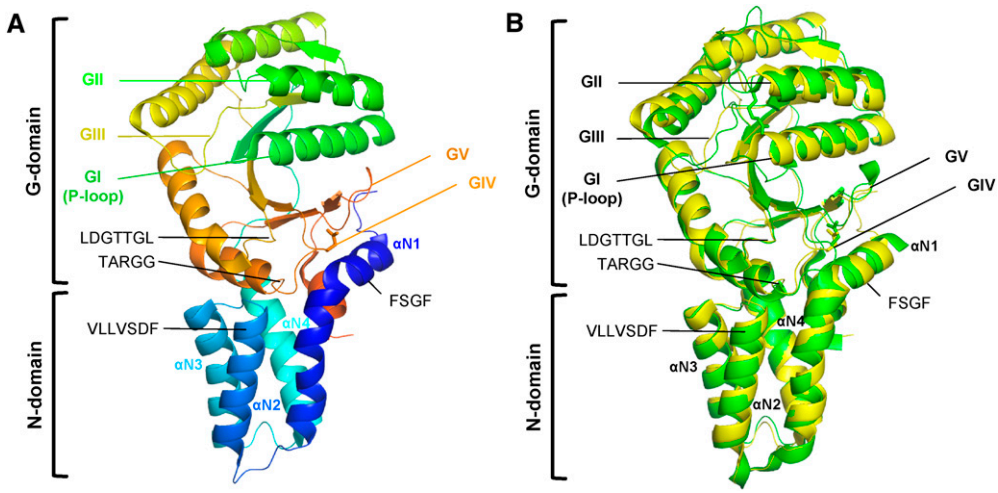

Figure 8. Crystal Structure of *P. patens* cpFtsY and Structural Comparison with *Arabidopsis* cpFtsY.

(A) The α-helices of the N-domain (αN1 to αN4) of Pp-cpFtsY are depicted in shades of blue. The G-domain including the GI-GV motifs are colored green, yellow, and orange. Conserved sequences at the NG interface (^{85}FSGF^{88}, ^{120}VLLVSDF^{126}, ^{308}LDGTTGL^{314}, and ^{340}TARGG^{344}) are marked in black. The conserved Asp residue Asp-338 of the GIV motif is shown as a stick model.

(B) Superposition of the chloroplast FtsY structures of *P. patens* (yellow) and *Arabidopsis* (green; 2OG2). The conserved Asp residues (Pp-D338 and At-D283) of the GIV motif as well as the conserved Arg (lacking in Pp-cpFtsY; At-R166) in the GII motif are shown as sticks.

a consequence of the P-loop conformation. Notably, in both available At-cpFtsY structures, a malonate resulting from the crystallization buffer occupies the P-loop and coordinates several residues, including the Arg of the GII motif.

The GIV motif harbors the highly conserved TKLD motif in which the Asp residue has a special relevance for the coordination of the guanidine moiety of the bound nucleotide (Figures 9A and 9C). Besides the position of the αN2 helix within the N-domain, the position of Asp-283 within the GIV motif of the At-FtsY is critical for its closed structure. In contrast with bacterial FtsY, the Asp residue of the free noncomplexed At-cpFtsY (Asp-283) is shifted toward the guanine base in the binding pocket, which leads to a decreased distance and enhanced nucleotide specificity (Jaru-Ampornpan et al., 2007; Chandrasekar et al., 2008). A comparable Asp position and distance of ~2.5 Å to the guanine base was otherwise only observed for Ta-FtsY in complex with Ta-Ffh (Figure 9C; Reyes et al., 2007). In cpFtsY of *P. patens*, the corresponding residue Asp-338 is positioned like the Asp-356 of the apo prokaryotic Ta-FtsY. Distances of 4.0 and 3.3 Å between the conserved Asp and the guanine base were determined for Pp-cpFtsY and for free Ta-FtsY, respectively (Figure 9C; Reyes et al., 2007). Hence, our data show that the catalytically essential Asp-338 of Pp-cpFtsY is not positioned as described for cpFtsY of *Arabidopsis* (Chandrasekar et al., 2008) but remains withdrawn as it is described for several prokaryotic apo-FtsY structures (Montoya et al., 1997; Gariani et al., 2006; Parlitz et al., 2007; Reyes et al., 2007).

Taken together, the overall structure of Pp-cpFtsY resembles the closed structure of At-cpFtsY. Nevertheless, the uncommon P-loop conformation and the prokaryotic feature of the Asp residue Asp-338 within the GIV motif indicate significant differences in the nucleotide binding pocket.

The Nucleotide Specificity of *P. patens* cpFtsY Is More Related to That of Higher Plant Chloroplast FtsY Than to That of Prokaryotic FtsY

To be able to compare the biochemical characteristics of *P. patens* cpFtsY with the corresponding *Arabidopsis* and *E. coli* proteins, we determined the nucleotide affinity of Pp-cpFtsY and the mutant Pp-cpFtsY(D338N) toward cognate and noncognate nucleotides by isothermal titration calorimetry (ITC). Previously, it was shown that the Asp-to-Asn mutation converts At-cpFtsY, as many other GTPases, from a GTP to an XTP-specific protein with a switch in nucleotide specificity of 40- to 250-fold (Jaru-Ampornpan et al., 2007). By contrast, wild-type and mutant *E. coli* FtsY show no more than a twofold discrimination between nucleotides, and nucleotide specificity is only achieved upon complex formation with Ffh (Shan and Walter, 2003).

To circumvent the effect of measuring mixed GTP and GDP affinities, which would occur due to GTP hydrolysis catalyzed by the proteins, we performed ITC measurements with GDP and XDP as these nucleotides are bound with similar affinities compared with the corresponding nucleoside triphosphates (Shan and Walter, 2003; Jaru-Ampornpan et al., 2007). Pp-cpFtsY preferentially binds GDP, as K_d values of 9 and 50 μM for GDP and XDP were determined, respectively (Table 1, Figure 10). A detailed collection of the ITC data is shown in Supplemental Table 3 online. The D338N mutation in Pp-cpFtsY resulted in a preferential binding of XDP (K_d value: 7.5 μM) versus GDP (K_d value: 534 μM). The K_d value for GDP is in the same range as was previously described for At-cpFtsY (K_d value: 3.1 μM) and *E. coli* FtsY (K_d value: 24 μM) (Shan and Walter, 2003; Jaru-Ampornpan et al., 2007).

Our results show that, like the *Arabidopsis* protein, *P. patens* cpFtsY has a high specificity for guanine-based nucleotides.

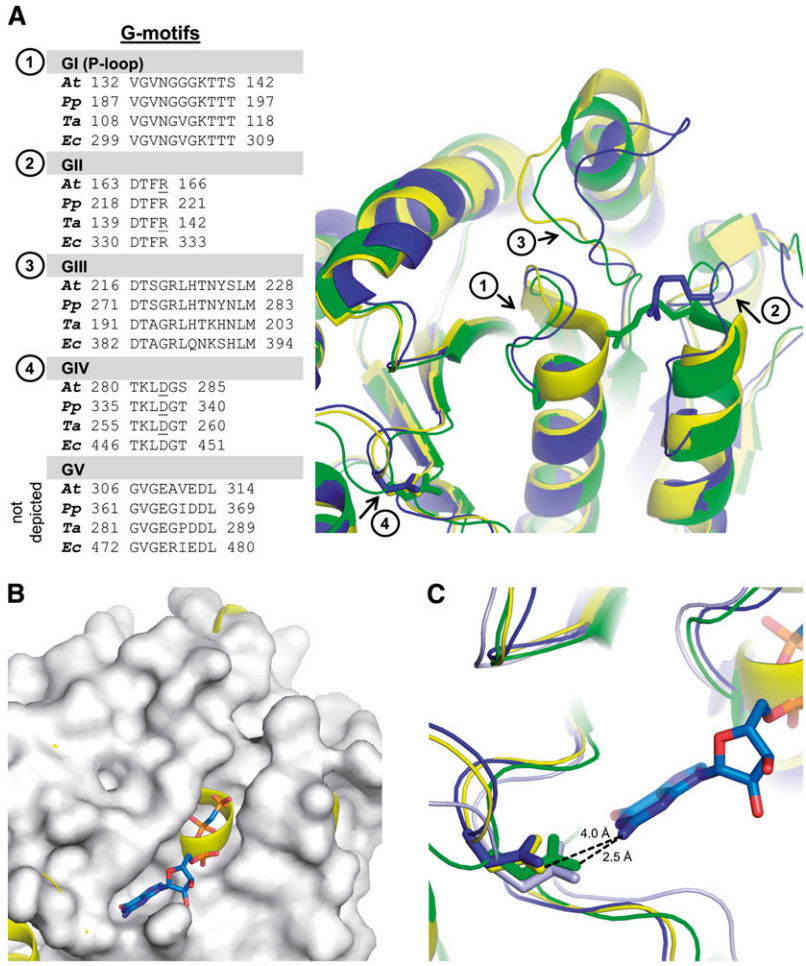

Figure 9. The G-Domain of *P. patens* cpFtsY.

(A) Comparison of the conserved G-motifs within the G-domain of apo-(cp)FtsY structures. Left: Alignments of the G-motifs from different organisms show high sequence conservation. Right: Structure of the G-motifs in cartoon representation. Residues shown as sticks are underlined in the alignment. The *P. patens* structure exhibits a different GI motif (P-loop) conformation. Two residues (Phe-220/Arg-221) within the GII motif are not resolved. *At*, *Arabidopsis* (green, 2OG2); *Pp*, *P. patens* (yellow); *Ta*, *T. aquaticus* (dark blue, 2Q9A); *Ec*, *E. coli*, structure not depicted. The GV motif is not illustrated. **(B)** View onto the nucleotide binding pocket of Ta-FtsY superimposed with the Pp-cpFtsY structure. Shown is the *T. aquaticus* FtsY (white, surface representation) of the Ta-FtsY-Ffh complex (1OKK) with bound nucleotide analog GCP (in stick representation). Superimposed onto this structure is the *P. patens* cpFtsY (yellow). Due to the P-loop conformation of Pp-cpFtsY, a part of the α-helix of the GI motif occupies the binding pocket, making nucleotide binding impossible without any structural changes.
(C) Comparison of GIV motifs. Shown are the GIV motifs of different (cp)FtsY structures. The guanine moiety coordinating Asp residues (Pp-D338; At-D283; Ta-D356) are depicted as sticks. Distances toward the guanine base for apo (3.3 Å) and complexed (2.7 Å) Ta-FtsY had been measured earlier (Reyes et al., 2007). In contrast with the *Arabidopsis* Asp residue, which is positioned as in the complexed Ta-FtsY, the *P. patens* residue remains withdrawn as observed for the free form of Ta-FtsY. Pp-cpFtsY (yellow); At-cpFtsY (green, 2OG2); Ta-FtsY (dark blue, 2Q9A); *T. aquaticus* Ffh-FtsY complex with GCP (light blue, 1OKK).

However, the 8- to 60-fold discrimination between wild-type and mutant Pp-cpFtsY for GDP versus XDP is significantly lower than described for At-cpFtsY.

DISCUSSION

Here, we present a thorough analysis of the phylogenetic distribution of SRP components in photosynthetic organisms and a molecular characterization of the SRP system in *P. patens* as the first example of a land plant harboring all components of the classical bacterial SRP system and the chloroplast-specific cpSRP43 component.

Phylogenetic Distribution, Structure, and Function of Plastid SRP RNA

The finding of plastid-encoded SRP RNA genes in many of the lineages of photosynthetic organisms show that all the

Table 1. Nucleotide Dissociation Constants (K_d) for Wild-Type and Mutant Pp-cpFtsY Determined by ITC

Construct	K_d (μM)	
	GDP	XDP
cpFtsY	9 ± 1.5	50 ± 10
cpFtsY(D338N)	534 ± 50	7.5 ± 0.8

The average and SD were calculated from double or triple determinations. For further details, see also legend of Figure 10 and Supplemental Table 3 online.

components of the bacterial-type cotranslational SRP pathway are conserved in many more organisms than previously thought. However, we also show that the plastid SRP RNA has been subject to parallel losses during evolution, as previously shown for many other plastid genes (Martin et al., 1998).

All identified plastid SRP RNAs in the red group as well as basal green algae conform to the standard bacterial SRP RNA with very few small deviations. In other green algae and land plants, the conserved region is much more variable, especially the apical loop display variants not found in bacterial SRP RNAs (Rosenblad et al., 2009). Other deviations from the bacterial consensus were larger asymmetrical loops and less clear secondary structure predictions in the less conserved parts of the SRP RNA (Figure 4A; see Supplemental Figure 1 online). However, the similarity within the different phylogenetic groups is very high, and the plastid SRP RNA is found in conserved genomic locations in most of the species examined (Figure 2; see Supplemental Figure 2 online). These data point to the plastid SRP RNA being an important component of the plastid SRP. Nevertheless, deviations in most green plant cpSRP RNAs from bacterial SRP RNAs raise doubts about what functions these cpSRP RNAs perform. Here, we show that the ability of *P. patens* cpSRP RNA to enhance GTP hydrolysis by the SRP GTPases Ffh/cpSRP54 and (cp)FtsY is drastically reduced, which might be due to the elongated apical loop (Figure 7). In bacteria, the regulation of the GTPase cycle plays an important role for the coordination of substrate delivery and release at the SecY translocase (Shan et al., 2007; Zhang et al., 2009), which leads to the assumption that other biological factors might compensate for functional loss of the SRP RNA in chloroplasts. An influence of cpSRP43 and the thylakoid membrane Alb3 translocase on the GTPase activity has been reported for higher plants (Goforth et al., 2004; Lewis et al., 2010). An unresolved question is whether the cpSRP RNA has a role in catalyzing the complex formation between cpSRP54 and cpFtsY as was shown for the bacterial system (Peluso et al., 2000, 2001; Bradshaw et al., 2009). For cpSRP systems containing SRP RNAs that do not deviate from the consensus bacterial SRP structure, it is feasible that a mechanism similar to the transient tether model explaining enhanced complex formation in bacteria applies (Shen and Shan, 2010). Here, a highly conserved Lys residue in FtsY plays a crucial role for acceleration of complex formation by providing a receptor for the tetra loop RNA. However, this model is not completely transferable to the chloroplast system as the critical Lys residue is not conserved. Applying the transient tether model to the SRP system of organisms containing SRP

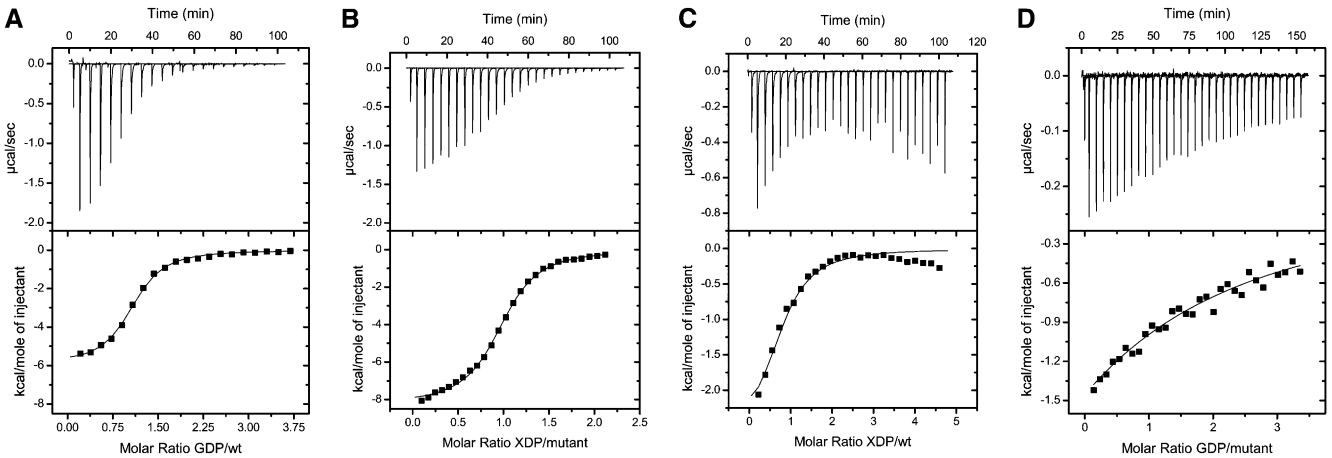

Figure 10. Determination of Nucleotide Binding Affinities of Pp-cpFtsY and Pp-cpFtsY(D338N) by ITC.

Nucleotide was injected stepwise into protein solution, and the resulting changes in heating power were recorded (top panels). After integration, the resulting enthalpy changes are plotted versus the molar ratio of nucleotide and protein (bottom panels). The following concentrations were used in the syringe and the cell, respectively: **(A)** 3 mM GDP and 158 μM wild-type (wt) Pp-cpFtsY; **(B)** 1.4 mM XDP and 142 μM mutant Pp-cpFtsY(D338N); **(C)** 4 mM XDP and 177 μM wild-type Pp-cpFtsY; **(D)** 2 mM GDP and 120 μM mutant Pp-cpFtsY(D338N). The curves were fitted to the data according to a one-site binding model, yielding the results shown in Table 1 and Supplemental Table 3 online.

RNAs with elongated apical loops is even more difficult. Furthermore, analysis of the crystal structure of *P. patens* cpFtsY shows that it has a closed conformation similar to the one of *Arabidopsis*, which indicates that no significant structural rearrangements are required during complex formation with cpSRP54 (Figure 8). The closed conformation of *P. patens* cpFtsY was further supported by analyzing its nucleotide specificity (Table 1). Although the highly conserved Asp within the GIV motif of *P. patens* cpFtsY is positioned as in other prokaryotic FtsY apo-structures, the nucleotide specificity of *P. patens* cpFtsY and the mutant protein cpFtsY (D338N) is more similar to *Arabidopsis* cpFtsY than to prokaryotic FtsY (Shan and Walter, 2003; Jaru-Ampornpan et al., 2007). Furthermore, these data suggest that the position of the Asp residue within the GIV motif is not the only factor determining the nucleotide specificity. However, it cannot be ruled out that the Asp residue is flexible without any bound nucleotide; therefore, crystallization of nucleotide-loaded cpFtsY from *P. patens* and *Arabidopsis* will be necessary to clarify the significance of the Asp position.

The finding that the preformed closed conformation of cpFtsY is not phylogenetically correlated to the loss of the cpSRP RNA indicates that this conformational change of cpFtsY is not sufficient to enable an efficient cpFtsY/cpSRP54 complex formation. Interestingly, it has been shown that in *Arabidopsis* the M-domain of cpSRP54 mimics the function of the SRP RNA by providing a significant acceleration of complex formation between the cpSRP GTPases (Jaru-Ampornpan et al., 2009). This leads to the speculation that the M-domain of *P. patens* cpSRP54 might still resemble the classic bacterial M-domain, which has no stimulating influence on complex formation (Jaru-Ampornpan et al., 2009) and might therefore still depend on an SRP RNA for efficient cpFtsY binding.

The P-Loop Structure of *P. patens* cpFtsY Is Similar to the apo Form of *M. mycoides* FtsY

The GI loop (P-loop) is involved in positioning the α- and β-phosphate groups of the substrate GTP. Although the sequence is highly identical between Pp-cpFtsY and At-cpFtsY within the P-loop region, the observed structure for the P-loop of *P. patens* apo-cpFtsY is markedly different to both apo-structures described for *Arabidopsis* cpFtsY (Stengel et al., 2007; Chandrasekar et al., 2008) and to the apo-structure of bacterial FtsY from *E. coli* (Montoya et al., 1997; Parlitz et al., 2007) and *T. aquaticus* (Reyes et al., 2007) (Figures 9A and 9B). However, as in both described At-cpFtsY structures, a negatively charged malonate ion is bound to the P-loop, which mimics the α- and β-phosphate groups of a nucleotide, an influence on the P-loop conformation cannot be completely ruled out. Interestingly, the P-loop conformation of Pp-cpFtsY is similar to the apo-form of *M. mycoides* (Mm) FtsY but differs to the sulfate-loaded form of Mm-FtsY, which exhibits the same P-loop conformation as described for other bacterial and chloroplast (cp)FtsY proteins (Gariani et al., 2006). It is possible that three subsequent Gly residues within the P-loop, which are unique to most chloroplast FtsY proteins and probably increase the flexibility in this region (Stengel et al., 2007), contribute to the observed P-loop conformation. Furthermore, as no ligand is bound to the P-loop this might also increase the flexibility in this region. Therefore, our data support the view of Gariani et al. (2006) suggesting an intrinsic mobility of the P-loop that enables a switch between two conformations. As one conformation prevents nucleotide binding, this might explain the low affinity of FtsY for GTP and the low basal GTP hydrolysis activity (see Gariani et al. [2006] and the discussion herein).

Phylogenetic Distribution of Plastid SRP54 and SRP43

Our analysis of plastid SRP54 sequences showed a strong correlation between a lack of plastid SRP RNA and mutations in the SRP RNA binding positions (Figure 1; see Supplemental Table 1 online). Importantly, this is also the case in the red lineage. Observed mutations in the green and red lineages were S455[VA] and S455[VFQ], and G480[EDA] and G480[DAF], respectively, using the *Arabidopsis* positions as reference (see Supplemental Figure 5 online). It is not clear why these mutations evolved when there was no plastid SRP RNA to bind to. One reason could be that the plastid SRP RNA during evolution had mutated to be nonfunctional or even detrimental, so that it became necessary for the plastid SRP54 not to bind to it.

Another question is why these mutations are almost universally retained when the plastid SRP RNA has been lost. The G480E/D and the S455A change requires only one nucleotide mutation, so back-mutations are easily accomplished. However, in all seed plant cpSRP54 sequences, including ESTs, we have only found one example of a nonmutated RNA binding position: a conserved SM motif in *Gingko* ESTs (see Supplemental Figure 5 online). Furthermore, one would expect a greater variability in the mutations if the amino acids no longer had a clear function. Still, it is possible that the changes are also part of a transition in cpSRP54 structure and, thus, not only there to abolish the RNA binding. Regarding the two organisms (*Pteridium* and *Chaetosphaeridium*) that had both a cpSRP RNA and a cpSRP54 with a mutated RNA binding domain, it is possible that the cpSRP RNA cannot bind to cpSRP54 and thus does not participate in any of the cpSRP pathways.

The cpSRP43 analysis showed that the previous assumption that plastids either contain a plastid SRP RNA or cpSRP43 is not supported by our data as all green organisms with a cpSRP RNA also have cpSRP43 candidates. Some of the candidate cpSRP43s in green algae have no identified chromo domain 1 (CD1) (see Supplemental Figure 6 online). Although this seems to indicate a lack of function, as higher plant CD1 mutants do not support integration of LHCP (Goforth et al., 2004), no experiments have so far been performed with green algae components. In fact, there is still no evidence that the posttranslational cpSRP of green algae functions in the same way as in higher plants. Until these questions have been resolved, the cpSRP43 candidates should be regarded as homologs, especially as they all have the critical CD2 domain. Another question is whether the cpSRP43 proteins of land plants, which have a cpSRP RNA, can bind to a cpSRP54/cpSRP RNA particle. Here, we showed that *P. patens* cpSRP54 binds both the cpSRP RNA and cpSRP43 (Figure 6). However, currently it is not known whether cpSRP54 can bind both components simultaneously. It is possible that the cpSRP RNA binds only loosely to cpSRP54 and is released

when cpSRP54 binds to cpSRP43 to form the posttranslational cpSRP. In this scenario, the function of cpSRP RNA might be restricted to the cotranslational SRP pathway. However, it is also possible that cpSRP54 bound to the cpSRP RNA is not able to interact with cpSRP43. Then, the cpSRP54/cpSRP RNA particle might play a role in cotranslational protein transport and the posttranslational targeting of LHCP is mediated by cpSRP43 only. This is conceivable because it was shown that cpSRP43 is sufficient to prevent aggregation of the hydrophobic LHCP (Falk and Sinning, 2010; Jaru-Ampornpan et al., 2010). Furthermore, an in vivo study indicated that cpSRP43 can function independently of cpSRP54/cpFtsY in mutants lacking these components (Tzvetkova-Chevolleau et al., 2007). However, targeting mechanisms might also be flexible using various SRP components.

In conclusion, detailed molecular studies of the SRP pathways of various green organisms are necessary to further understand the evolution from the prokaryotic to the higher plant chloroplasts SRP pathway. With protein sequences now available for SRP GTPases of species other than green plants, it will be interesting to compare the evolution and function of these to the SRP GTPases of the green lineage. As the loss of the plastid SRP RNA has occurred several times during evolution, it is possible that nature has found more than one solution to an RNA-less SRP pathway.

METHODS

Sources of Plastid Genome Sequences

A total of 130 plastid genomes (complete or partial sequences) were searched, excluding angiosperms but including four gymnosperms (for a complete list, see Supplemental Table 1 online).

Identification of SRP RNA Sequences and Prediction of RNA Secondary Structure

SRP RNA genes were predicted as described previously (Regalia et al., 2002) and also by extracting candidate sequences using FASTA36 with a word size of 3 or cmsearch in local mode (Infernal v. 0.81) with the Rfam 9 RF00169.cm model (http://rfam.sanger.ac.uk/). Candidates were only considered if they displayed all of the most conserved features of SRP RNAs and mapped to intergenic regions. In no case did we identify the similarly structured 4.5 S rRNA of land plants, representing the 3′ of the uncleaved 23 S pre-rRNA, as a plastid SRP RNA candidate. Noncanonical changes were accepted in the helix eight apical loop according to known variability (Rosenblad et al., 2009 and M.A. Rosenblad, unpublished data) or if the change was highly conserved (e.g., a much longer apical loop in land plants). RNA secondary structure predictions were performed by cmsearch (Infernal v. 0.81) (Nawrocki et al., 2009) and MFOLD (Zuker, 2003), sometimes using constraints to guide the folding according to the consensus conserved part. Multiple alignments of RNA primary sequences were made with ClustalW and cmalign (Infernal). The complete nucleotide database at NCBI was furthermore searched for homologs using NCBI BLASTN with a word size of 7 and low complexity filtering turned off, with predicted plastid SRP RNAs as queries. Upstream putative promoter sequences were predicted by comparison to previously published plastid SRP RNAs and cyanobacterial RNA genes. Gene order was extracted from published plastid genomes, with nonconserved open reading frames in some cases removed (*Cyanidioschyzon*) and a few unannotated genes added (*psbX*, *Cyanidium*; *petN*, *Marchantia*). All predicted RNA sequences and multiple alignments are shown in Supplemental Figure 1 online.

Identification of Plastid SRP54 and SRP43

Published plastid SRP54 and SRP43 sequences were used in BLASTP searches versus the NCBI nonredundant protein database and predicted proteins from genome projects, as well as TBLASTN searches versus NCBI dbEST, genome project EST, and genome databases. Candidates considered were compared with the plastid protein homologs as well as bacterial and cytoplasmic Ffh/SRP54 homologs to ensure their identity as plastid proteins. The RNA binding region of plastid SRP54 was extracted from a multiple alignment of the found sequences made by ClustalW2 (Goujon et al., 2010), implemented into GeneDoc and essential positions were marked. The cpSRP43 sequences were identified in a similar way, and domain organization was predicted using SMART, PROSITE, and Pfam databases. For *Chlamydomonas reinhardtii* cpSRP43, RT-PCR was performed since the published sequence lacked domains considered to be part of the cpSRP43 architecture (see below). In a few cases, the cpSRP43 gene prediction was reevaluated using closely related homologs and EST data. The accession numbers for the analyzed protein sequences are found in Supplemental Table 1 online. For many of the organisms, protein sequence data was not available.

Identification of *C. reinhardtii* cpSRP43 by RT-PCR

The isolation of RNA from *C. reinhardtii* cells (2×10^6 cells per mL) was done by the peqGOLD TriFast method (PeqLab), and the mRNA was isolated from total RNA extract using the Oligotex mRNA mini kit (Qiagen) both according to the manufacturer's instructions. For the RT-PCR reactions, the One-Step RT-PCR kit (Qiagen) was used also according to the manufacturer's instructions. Received RT-PCR products were subcloned and verified by sequencing. The cDNA sequence encoding full-length cpSRP43 was assembled from partial sequences.

Plasmid Construction

Sequences for cloning were amplified using proofreading KOD DNA polymerase (Novagen). For radiolabeled in vitro translation, full-length *Escherichia coli* Ffh and *Arabidopsis thaliana* cpSRP54 (amino acids 75 to 564) were cloned into pIVEX1.3WG plasmid (Roche) introducing a C-terminal stop codon and using *Nco*I-*Sal*I restriction sites. For yeast two-hybrid analyses, the plasmid pACT2 (Clontech/Takara Bio) was used to construct the *Physcomitrella patens* cpSRP43 prey plasmid. This construct encoded amino acids 185 to 419 of full-length cpSRP43, which corresponds to the sequence encoded by the longest available cpSRP43-cDNA clone (pp020045322r). Amplified DNA was cloned into pACT2 using the restriction enzymes *Nco*I-*Pag*I and *Eco*RI. Plasmid pGBKT7 (Clontech/Takara Bio) was used as bait plasmid, and *P. patens* cpSRP54 (amino acids 126 to 617) was inserted into the *Nco*I-*Sal*I restriction sites. For gel filtration analyses, the coding sequence of mature *P. patens* cpSRP43 (62 to 419) and a truncation construct (174 to 419, lacking the first chromo domain) were cloned (*Bam*HI-*Sal*I) into the pETDUET-1 plasmid (Novagen), facilitating expression with an N-terminal 6x-His-tag. These cDNAs were generated by overlap PCR using the available cDNA clone (pp020045322r) and a cDNA sequence coding for the predicted N-terminal region (1 to 184 amino acids), which had been synthesized and cloned into a pUC-57 plasmid (GenScript). The coding sequence for mature *P. patens* cpSRP54 (amino acids 126 to 617) was cloned into pET-29b(+) (Novagen) using the *Nco*I-*Sal*I restriction sites for expression with C-terminal His tag. Additionally, for GTPase activity measurements, the coding sequence for full-length *E. coli* Ffh was cloned into pET-29b(+) (Novagen) using the *Nco*I-*Sal*I restriction sites for expression with C-terminal His tags. The coding sequence for *P. patens* cpFtsY was synthesized in an optimized form, adjusted for expression in *E. coli* according to its codon usage (GenScript). Using *Bam*HI-*Sal*I restriction sites, the cpFtsY (amino acids 57 to 383) coding sequence was cloned into the pETDUET-1 plasmid (Novagen), facilitating expression with an N-terminal

6x-His-tag. The constructs for expression of the mature forms of *Arabidopsis* cpSRP54 and cpFtsY with N-terminal His-tags and of *E. coli* His-FtsY were described by Bals et al. (2010) and Luirink et al. (1994), respectively. For crystallization, *P. patens* cpFtsY (amino acids 80 to 383) was cloned into the pETDUET-1 plasmid (Novagen) using *Bam*HI-*Sal*I restriction sites. To generate the mutant construct *P. patens* cpFtsYΔ1-79(D338N) for ITC measurements, the QuikChange XL site-directed mutagenesis kit (Agilent Technologies) was used according to the manufacturer's instructions and the pETDUET-1-Pp-cpFtsYΔ1-79 plasmid served as template. In each case, the correctness of the constructs was verified by sequencing. DNA coding for *P. patens* cpSRP RNA was synthesized and cloned into pUC-57 plasmid (GenScript).

In Vitro Transcription and Translation

To generate RNA for structure probing, binding assays, and GTPase activity assays, DNA coding for *E. coli* SRP RNA (Schuenemann et al., 1999), *P. patens* cpSRP RNA, and *Ostreococcus* cpSRP RNA (Richter et al., 2008) were amplified by template-specific primers, where the forward primers contained the T7-promoter sequence. Proofreading PRECISOR High-Fidelity DNA Polymerase (Biocat) was used. These PCR products were used for run-off in vitro transcription with the TranscriptAid T7 high-yield transcription kit (Fermentas) according to the manufacturer's instructions. RNA was purified using mini Quick Spin RNA Columns (Roche) according to the manufacturer's instructions, and RNA yields were determined using NanoDrop 2000c (Thermo Scientific). RNA sizes were checked using 10% polyacrylamide gels and ethidium bromide stain.

Using the RTS 100 Wheat Germ CECF kit (Roche) according to the manufacturer's protocol, the pIVEX1.3WG constructs of *E. coli* Ffh, *Arabidopsis* cpSRP54, and *P. patens* cpSRP54 (Richter et al., 2008) were transcribed and radiolabeled with [^{35}S]Met (Hartmann Analytic) during translation.

Structure Probing

A total of 30 pmol of in vitro–transcribed *P. patens* cpSRP RNA was treated as described previously (Brantl and Wagner, 1994). Briefly, RNA was dephosphorylated using calf intestinal alkaline phosphatase (Fermentas), phenol-extracted, and precipitated. T4 Polyribonucleotide Kinase (Fermentas) facilitated 5′-end labeling with [γ-^{32}P]ATP (Hartmann Analytic). The 5′-end–labeled RNA was gel purified and extracted. Experiments for partial digestion of the 5′-end–labeled RNA were done according to Waldminghaus et al. (2009) using RNase T1 (0.002 , 0.005, and 0.01 units at 30°C and 0.01 units at 45°C; Ambion). RNA fragments were separated on denaturing 8% polyacrylamide gels.

RNA Binding Assay and Yeast Two-Hybrid Analyses

RNA binding assays were conducted as described previously (Richter et al., 2008). Constructs used for protein–protein interactions in yeast two-hybrid analyses were either cloned in this study or published earlier (Jonas-Straube et al., 2001; Funke et al., 2005; Richter et al., 2008). Experiments were conducted as described previously (Jonas-Straube et al., 2001; Funke et al., 2005).

Gel Filtration Chromatography

His-tag fusion proteins were expressed in *E. coli* Rosetta(DE3)pLysS (Novagen). Purification of *P. patens* cpSRP43 constructs was achieved using nickel-nitrilotriacetic acid agarose (Qiagen), and *P. patens* cpSRP54 purification was achieved using 5 mL of His-Trap HP (GE Healthcare) with ÄKTApurifier. All proteins were eluted with elution buffer (20 mM $NaPO_4$, 500 mM NaCl, 500 mM imidazole, and 2 mM DTT, pH 7.4). Subsequently, they were transferred into column buffer (25 mM HEPES NaOH, pH 8.0, 200 mM NaCl, 5 mM $MgCl_2$, 5% (v/v) glycerol, and 2 mM DTT) using PD-10 columns (GE Healthcare) or Superdex75 10/300 GL (GE Healthcare). A total of 7 nmol of each component was mixed and incubated for 15 min at 4°C by rotating end over end before loading onto Superdex200 10/300 GL (GE Healthcare). Gel filtration analysis was performed in column buffer at a flow rate of 0.4 mL/min. Reference runs were performed with the individual proteins.

Assay of GTPase Activity

His tag fusion proteins were expressed in *E. coli* Rosetta(DE3)pLysS (Novagen) and purified using nickel-nitrilotriacetic acid agarose (Qiagen). Proteins were eluted with elution buffer (25 mM HEPES NaOH, pH 8.0, 150 mM NaCl, 10 mM $MgCl_2$, and 250 mM imidazole).

GTPase activity assays were performed as described previously (Goforth et al., 2004) with the following modifications: All reactions contained 200 pmol of each indicated protein, 0.01% Nikkol ($C_{12}E_8$; Sigma-Aldrich), 5 mM GTP, and 1 μL RiboLock RNase Inhibitor (Fermentas) in samples containing RNA (threefold molar excess).

Expression and Purification of *P. patens* cpFtsY for Crystallization

For cpFtsY crystallization, the pETDUET-1-Pp-cpFtsYΔ1-79 plasmid was expressed and purified as described above using the following elution buffer: 25 mM HEPES NaOH, pH 8.0, 150 mM NaCl, 250 mM imidazole, and 2 mM DTT. Further purification of Pp-cpFtsY was accomplished by size exclusion chromatography using ÄKTApurifier at a flow rate of 0.25 mL/min and a Superdex75 10/300 GL column (GE Healthcare) with gel filtration buffer (25 mM HEPES NaOH, pH 8.0, 150 mM NaCl, and 2 mM DTT).

Crystallization, Data Collection, and Structure Determination

P. patens cpFtsY was concentrated to 8 to 15 mg/mL and supplemented with 5% (v/v) glycerol. Crystallization conditions were screened (18°C, dark) by the sitting drop vapor diffusion method using the Classics Suite, the Classics II Suite, the Cryo Suite, the JCSG+ Suite, the MbClass II Suite, the MbClass Suite, the PACT Suite, the PEGs II Suite, and the PEGs Suite (all Qiagen), applying 200/100- and 100/100-nL mixtures of the protein/reservoir solution. After 3 weeks, a single crystal with the approximate dimensions of 110 μm × 55 μm × 25 μm was obtained in 0.2 M sodium nitrate, 0.1 M bis-tris propane, pH 6.5, and 20% (w/v) polyethylene glycol 3350. The crystal was soaked in mother liquor supplemented with 30% polyethylene glycol 400 before flash-cooling in liquid nitrogen. Oscillation data were collected to a resolution of 1.8 Å at the Swiss Light Source (Villigen, Switzerland) on beamline PXII at 100K using a Pilatus 6M detector. Processing and scaling of data were done using the XDS program package (Kabsch, 2010). Pp-cpFtsY crystallizes in space group $P2_12_12$, with two molecules per asymmetric unit and a solvent content of 47%. The structure was solved by molecular replacement using PHENIX (Adams et al., 2010) with *Arabidopsis* cpFtsY (Protein Data Bank code 2OG2) as search model. The structure was refined using iterative cycles of manual rebuilding in COOT (Emsley and Cowtan, 2004) and automatic refinement using PHENIX (Adams et al., 2010). Noncrystallographic symmetry restraints were used throughout the refinement and were only released for selected residues differing in conformation between the two copies. Illustrations were generated with PYMOL (www.pymol.org). The model has been deposited at the Protein Data Bank under accession number 4AK9.

ITC

All proteins used for ITC measurements were expressed as described above using the following elution buffer (25 mM HEPES NaOH, pH 8.0, 150 mM NaCl, 5mM $MgCl_2$, 250 mM imidazole, and 2 mM DTT). Further

purification of the proteins was accomplished by size exclusion chromatography using ÄKTApurifier (GE Healthcare) with the same settings as described above, in ITC buffer (25 mM HEPES NaOH, pH 8.0, 150 mM NaCl, 5 mM $MgCl_2$, 2 mM DTT, 0.01% Nikkol [$C_{12}E_8$; Sigma-Aldrich], and 5% [v/v] glycerol).

All ITC experiments were performed in ITC buffer at 30°C using a Microcal AutoITC200 (GE Healthcare). The sample cell was filled with 120 to 250 μM of protein and was titrated to a two- to fivefold excess of nucleotide by 21 or 32 injection steps of 1.8 or 1.2 μL, each using 1.5 to 4.5 mM nucleotide. The concentration of the used GDP (Sigma-Aldrich) and XDP (Jena Biosciences) was determined by UV absorption at 254 nm [ε = 13,700 $(M \cdot cm)^{-1}$]. Control experiments were performed by titration of nucleotide solution into ITC buffer, resulting in small and constant background signals. ITC data were analyzed using ITC-Origin 7 (Microcal/GE Healthcare) according to the one-site binding model.

Accession Numbers

Accession numbers are given in Supplemental Table 1 online. For *Arabidopsis*, the following accession numbers were used: AAC64139 for cpSRP54 and NP_566101 for cpSRP43.

Supplemental Data

The following materials are available in the online version of this article.

Supplemental Figure 1. Plastid SRP RNA Alignments.

Supplemental Figure 2. Gene Order for All Plastid SRP RNA Regions.

Supplemental Figure 3. Promoter Sequences for All Organisms with Plastid SRP RNAs.

Supplemental Figure 4. Verification of Plastid SRP RNA Expression by RT-PCR in Different Lineages.

Supplemental Figure 5. Full Alignment of Plastid SRP54 Sequences.

Supplemental Figure 6. Domain Structure of cpSRP43 Proteins.

Supplemental Figure 7. Full Alignment of cpSRP43 Sequences.

Supplemental Figure 8. Phylogenetic Tree of Cytosolic SRα (SR) and Chloroplast FtsY (cpFtsY) Proteins.

Supplemental Figure 9. Alignment for Phylogenetic Tree Construction (Supplemental Figure 8).

Supplemental Table 1. Plastid SRP Component Identification Summary.

Supplemental Table 2. Summary of Crystallographic Data Collection and Structure Refinement Statistics.

Supplemental Table 3. ITC Data Collection of All Conducted Experiments.

Supplemental Methods 1.

Supplemental Data Set 1. Text File of Alignment Corresponding to Phylogenetic Analysis in Supplemental Figure 8.

ACKNOWLEDGMENTS

We thank Joen Luirink for kind gift of *E. coli* FtsY plasmid, the RIKEN Bioresource Center for full-length cDNA of Pp-cpSRP54 (Pdp05283), the staff at beamline PXII at the Swiss Light Source (Villigen, Switzerland) for help during data collection, and Stefan A. Rensing for providing the Pp-cpSRP43 sequence, the partial Pp-cpSRP43 cDNA clone (pp020045322r), wild-type *P. patens* ssp *patens* (Gransden 2004 strain), and valuable hints for cultivation of gametophytes. This work was supported by grants from the collaborative research center SFB 642 of the Deutsche Forschungsgemeinschaft (Teilprojekt A5 [C.H./K.K.], A22 [E.H.], and A23 [D.S.]), the Protein Research Department (D.S./E.H./C.T.), the Priority Program SPP 1258 of the Deutsche Forschungsgemeinschaft (F.N./B.K.), the Carl Tryggers Foundation (H.A./M.A.R.), the Swedish research council FORMAS (H.A.) and BILS (M.A.R.), the Studienstiftung des Deutschen Volkes (C.T.), and the Ruhr-University Research School (C.T./C.V.R.) funded by Germany's Excellence Initiative (DFG GSC 98/1).

AUTHOR CONTRIBUTIONS

D.S. and M.A.R. designed the research. C.T., D.Z., L.S., C.V.R., and C.G.-P. performed research. M.A.R., H.A., K.K., C.H., B.K., F.N., and E.H. contributed computational tools and other methods. C.T., M.A.R., and D.S. mainly analyzed data and wrote the article. All authors contributed partly to data analyses and article preparation.

Received July 31, 2012; revised December 7, 2012; accepted December 12, 2012; published December 28, 2012.

REFERENCES

Adams, P.D., et al. (2010). PHENIX: A comprehensive Python-based system for macromolecular structure solution. Acta Crystallogr. D Biol. Crystallogr. **66:** 213–221.

Amin, P., Sy, D.A., Pilgrim, M.L., Parry, D.H., Nussaume, L., and Hoffman, N.E. (1999). *Arabidopsis* mutants lacking the 43- and 54-kilodalton subunits of the chloroplast signal recognition particle have distinct phenotypes. Plant Physiol. **121:** 61–70.

Ataide, S.F., Schmitz, N., Shen, K., Ke, A., Shan, S.O., Doudna, J.A., and Ban, N. (2011). The crystal structure of the signal recognition particle in complex with its receptor. Science **331:** 881–886.

Bals, T., Dünschede, B., Funke, S., and Schünemann, D. (2010). Interplay between the cpSRP pathway components, the substrate LHCP and the translocase Alb3: An in vivo and in vitro study. FEBS Lett. **584:** 4138–4144.

Batey, R.T., Rambo, R.P., Lucast, L., Rha, B., and Doudna, J.A. (2000). Crystal structure of the ribonucleoprotein core of the signal recognition particle. Science **287:** 1232–1239.

Bradshaw, N., Neher, S.B., Booth, D.S., and Walter, P. (2009). Signal sequences activate the catalytic switch of SRP RNA. Science **323:** 127–130.

Brantl, S., and Wagner, E.G. (1994). Antisense RNA-mediated transcriptional attenuation occurs faster than stable antisense/target RNA pairing: An in vitro study of plasmid pIP501. EMBO J. **13:** 3599–3607.

Chandrasekar, S., Chartron, J., Jaru-Ampornpan, P., and Shan, S.O. (2008). Structure of the chloroplast signal recognition particle (SRP) receptor: Domain arrangement modulates SRP-receptor interaction. J. Mol. Biol. **375:** 425–436.

Dünschede, B., Bals, T., Funke, S., and Schünemann, D. (2011). Interaction studies between the chloroplast signal recognition particle subunit cpSRP43 and the full-length translocase Alb3 reveal a membrane-embedded binding region in Alb3 protein. J. Biol. Chem. **286:** 35187–35195.

Egea, P.F., Shan, S.O., Napetschnig, J., Savage, D.F., Walter, P., and Stroud, R.M. (2004). Substrate twinning activates the signal recognition particle and its receptor. Nature **427:** 215–221.

Emsley, P., and Cowtan, K. (2004). Coot: Model-building tools for molecular graphics. Acta Crystallogr. D Biol. Crystallogr. **60:** 2126–2132.

Falk, S., Ravaud, S., Koch, J., and Sinning, I. (2010). The C terminus of the Alb3 membrane insertase recruits cpSRP43 to the thylakoid membrane. J. Biol. Chem. **285:** 5954–5962.

Falk, S., and Sinning, I. (2010). cpSRP43 is a novel chaperone specific for light-harvesting chlorophyll a,b-binding proteins. J. Biol. Chem. **285:** 21655–21661.

Focia, P.J., Shepotinovskaya, I.V., Seidler, J.A., and Freymann, D.M. (2004). Heterodimeric GTPase core of the SRP targeting complex. Science **303:** 373–377.

Francis, M.A., Balint, R.F., and Dudock, B.S. (1987). A novel variety of 4.5 S RNA from *Codium fragile* chloroplasts. J. Biol. Chem. **262:** 1848–1854.

Franklin, A.E., and Hoffman, N.E. (1993). Characterization of a chloroplast homologue of the 54-kDa subunit of the signal recognition particle. J. Biol. Chem. **268:** 22175–22180.

Freymann, D.M., Keenan, R.J., Stroud, R.M., and Walter, P. (1997). Structure of the conserved GTPase domain of the signal recognition particle. Nature **385:** 361–364.

Funke, S., Knechten, T., Ollesch, J., and Schünemann, D. (2005). A unique sequence motif in the 54-kDa subunit of the chloroplast signal recognition particle mediates binding to the 43-kDa subunit. J. Biol. Chem. **280:** 8912–8917.

Gao, L., Zhou, Y., Wang, Z.W., Su, Y.J., and Wang, T. (2011). Evolution of the rpoB-psbZ region in fern plastid genomes: Notable structural rearrangements and highly variable intergenic spacers. BMC Plant Biol. **11:** 64.

Gariani, T., Samuelsson, T., and Sauer-Eriksson, A.E. (2006). Conformational variability of the GTPase domain of the signal recognition particle receptor FtsY. J. Struct. Biol. **153:** 85–96.

Goforth, R.L., Peterson, E.C., Yuan, J., Moore, M.J., Kight, A.D., Lohse, M.B., Sakon, J., and Henry, R.L. (2004). Regulation of the GTPase cycle in post-translational signal recognition particle-based protein targeting involves cpSRP43. J. Biol. Chem. **279:** 43077–43084.

Goujon, M., McWilliam, H., Li, W., Valentin, F., Squizzato, S., Paern, J., and Lopez, R. (2010). A new bioinformatics analysis tools framework at EMBL-EBI. Nucleic Acids Res. **38**(Web Server issue)**:** W695-W699.

Grudnik, P., Bange, G., and Sinning, I. (2009). Protein targeting by the signal recognition particle. Biol. Chem. **390:** 775–782.

Halic, M., Blau, M., Becker, T., Mielke, T., Pool, M.R., Wild, K., Sinning, I., and Beckmann, R. (2006). Following the signal sequence from ribosomal tunnel exit to signal recognition particle. Nature **444:** 507–511.

Holdermann, I., Meyer, N.H., Round, A., Wild, K., Sattler, M., and Sinning, I. (2012). Chromodomains read the arginine code of post-translational targeting. Nat. Struct. Mol. Biol. **19:** 260–263.

Hutin, C., Havaux, M., Carde, J.P., Kloppstech, K., Meiherhoff, K., Hoffman, N., and Nussaume, L. (2002). Double mutation cpSRP43 —/cpSRP54— is necessary to abolish the cpSRP pathway required for thylakoid targeting of the light-harvesting chlorophyll proteins. Plant J. **29:** 531–543.

Jaru-Ampornpan, P., Chandrasekar, S., and Shan, S.O. (2007). Efficient interaction between two GTPases allows the chloroplast SRP pathway to bypass the requirement for an SRP RNA. Mol. Biol. Cell **18:** 2636–2645.

Jaru-Ampornpan, P., Nguyen, T.X., and Shan, S.O. (2009). A distinct mechanism to achieve efficient signal recognition particle (SRP)-SRP receptor interaction by the chloroplast srp pathway. Mol. Biol. Cell **20:** 3965–3973.

Jaru-Ampornpan, P., Shen, K., Lam, V.Q., Ali, M., Doniach, S., Jia, T.Z., and Shan, S.O. (2010). ATP-independent reversal of a membrane protein aggregate by a chloroplast SRP subunit. Nat. Struct. Mol. Biol. **17:** 696–702.

Jonas-Straube, E., Hutin, C., Hoffman, N.E., and Schünemann, D. (2001). Functional analysis of the protein-interacting domains of chloroplast SRP43. J. Biol. Chem. **276:** 24654–24660.

Kabsch, W. (2010). Integration, scaling, space-group assignment and post-refinement. Acta Crystallogr. D Biol. Crystallogr. **66:** 133–144.

Klimyuk, V.I., Persello-Cartieaux, F., Havaux, M., Contard-David, P., Schuenemann, D., Meiherhoff, K., Gouet, P., Jones, J.D., Hoffman, N.E., and Nussaume, L. (1999). A chromodomain protein encoded by the *Arabidopsis* CAO gene is a plant-specific component of the chloroplast signal recognition particle pathway that is involved in LHCP targeting. Plant Cell **11:** 87–99.

Krissinel, E., and Henrick, K. (2007). Inference of macromolecular assemblies from crystalline state. J. Mol. Biol. **372:** 774–797.

Letsch, M.R., and Lewis, L.A. (2012). Chloroplast gene arrangement variation within a closely related group of green algae (Trebouxiophyceae, Chlorophyta). Mol. Phylogenet. Evol. **64:** 524–532.

Lewis, N.E., Marty, N.J., Kathir, K.M., Rajalingam, D., Kight, A.D., Daily, A., Kumar, T.K., Henry, R.L., and Goforth, R.L. (2010). A dynamic cpSRP43-Albino3 interaction mediates translocase regulation of chloroplast signal recognition particle (cpSRP)-targeting components. J. Biol. Chem. **285:** 34220–34230.

Luirink, J., High, S., Wood, H., Giner, A., Tollervey, D., and Dobberstein, B. (1992). Signal-sequence recognition by an *Escherichia coli* ribonucleoprotein complex. Nature **359:** 741–743.

Luirink, J., ten Hagen-Jongman, C.M., van der Weijden, C.C., Oudega, B., High, S., Dobberstein, B., and Kusters, R. (1994). An alternative protein targeting pathway in *Escherichia coli*: Studies on the role of FtsY. EMBO J. **13:** 2289–2296.

Martin, W., Stoebe, B., Goremykin, V., Hapsmann, S., Hasegawa, M., and Kowallik, K.V. (1998). Gene transfer to the nucleus and the evolution of chloroplasts. Nature **393:** 162–165.

Montoya, G., Svensson, C., Luirink, J., and Sinning, I. (1997). Crystal structure of the NG domain from the signal-recognition particle receptor FtsY. Nature **385:** 365–368.

Moore, M., Goforth, R.L., Mori, H., and Henry, R. (2003). Functional interaction of chloroplast SRP/FtsY with the ALB3 translocase in thylakoids: substrate not required. J. Cell Biol. **162:** 1245–1254.

Moore, M., Harrison, M.S., Peterson, E.C., and Henry, R. (2000). Chloroplast Oxa1p homolog albino3 is required for post-translational integration of the light harvesting chlorophyll-binding protein into thylakoid membranes. J. Biol. Chem. **275:** 1529–1532.

Nawrocki, E.P., Kolbe, D.L., and Eddy, S.R. (2009). Infernal 1.0: Inference of RNA alignments. Bioinformatics **25:** 1335–1337.

Nilsson, R., Brunner, J., Hoffman, N.E., and van Wijk, K.J. (1999). Interactions of ribosome nascent chain complexes of the chloroplast-encoded D1 thylakoid membrane protein with cpSRP54. EMBO J. **18:** 733–742.

Packer, J.C., and Howe, C.J. (1998). Algal plastid genomes encode homologues of the SRP-associated RNA. Mol. Microbiol. **27:** 508–510.

Parlitz, R., Eitan, A., Stjepanovic, G., Bahari, L., Bange, G., Bibi, E., and Sinning, I. (2007). Escherichia coli signal recognition particle receptor FtsY contains an essential and autonomous membrane-binding amphipathic helix. J. Biol. Chem. **282:** 32176–32184.

Peluso, P., Herschlag, D., Nock, S., Freymann, D.M., Johnson, A.E., and Walter, P. (2000). Role of 4.5S RNA in assembly of the bacterial signal recognition particle with its receptor. Science **288:** 1640–1643.

Peluso, P., Shan, S.O., Nock, S., Herschlag, D., and Walter, P. (2001). Role of SRP RNA in the GTPase cycles of Ffh and FtsY. Biochemistry **40:** 15224–15233.

Poritz, M.A., Bernstein, H.D., Strub, K., Zopf, D., Wilhelm, H., and Walter, P. (1990). An *E. coli* ribonucleoprotein containing 4.5S RNA resembles mammalian signal recognition particle. Science **250:** 1111–1117.

Powers, T., and Walter, P. (1997). Co-translational protein targeting catalyzed by the *Escherichia coli* signal recognition particle and its receptor. EMBO J. **16:** 4880–4886.

Regalia, M., Rosenblad, M.A., and Samuelsson, T. (2002). Prediction of signal recognition particle RNA genes. Nucleic Acids Res. **30:** 3368–3377.

Reyes, C.L., Rutenber, E., Walter, P., and Stroud, R.M. (2007). X-ray structures of the signal recognition particle receptor reveal targeting cycle intermediates. PLoS ONE **2:** e607.

Ribes, V., Römisch, K., Giner, A., Dobberstein, B., and Tollervey, D. (1990). *E. coli* 4.5S RNA is part of a ribonucleoprotein particle that has properties related to signal recognition particle. Cell **63:** 591–600.

Richter, C.V., Bals, T., and Schünemann, D. (2010). Component interactions, regulation and mechanisms of chloroplast signal recognition particle-dependent protein transport. Eur. J. Cell Biol. **89:** 965–973.

Richter, C.V., Träger, C., and Schünemann, D. (2008). Evolutionary substitution of two amino acids in chloroplast SRP54 of higher plants cause its inability to bind SRP RNA. FEBS Lett. **582:** 3223–3229.

Rosenblad, M.A., Larsen, N., Samuelsson, T., and Zwieb, C. (2009). Kinship in the SRP RNA family. RNA Biol. **6:** 508–516.

Rosenblad, M.A., and Samuelsson, T. (2004). Identification of chloroplast signal recognition particle RNA genes. Plant Cell Physiol. **45:** 1633–1639.

Saraogi, I., and Shan, S.O. (2011). Molecular mechanism of co-translational protein targeting by the signal recognition particle. Traffic **12:** 535–542.

Schuenemann, D., Amin, P., and Hoffman, N.E. (1999). Functional divergence of the plastid and cytosolic forms of the 54-kDa subunit of signal recognition particle. Biochem. Biophys. Res. Commun. **254:** 253–258.

Schuenemann, D., Gupta, S., Persello-Cartieaux, F., Klimyuk, V.I., Jones, J.D.G., Nussaume, L., and Hoffman, N.E. (1998). A novel signal recognition particle targets light-harvesting proteins to the thylakoid membranes. Proc. Natl. Acad. Sci. USA **95:** 10312–10316.

Shan, S.O., Chandrasekar, S., and Walter, P. (2007). Conformational changes in the GTPase modules of the signal reception particle and its receptor drive initiation of protein translocation. J. Cell Biol. **178:** 611–620.

Shan, S.O., and Walter, P. (2003). Induced nucleotide specificity in a GTPase. Proc. Natl. Acad. Sci. USA **100:** 4480–4485.

Shen, K., and Shan, S.O. (2010). Transient tether between the SRP RNA and SRP receptor ensures efficient cargo delivery during cotranslational protein targeting. Proc. Natl. Acad. Sci. USA **107:** 7698–7703.

Siu, F.Y., Spanggord, R.J., and Doudna, J.A. (2007). SRP RNA provides the physiologically essential GTPase activation function in cotranslational protein targeting. RNA **13:** 240–250.

Spanggord, R.J., Siu, F., Ke, A., and Doudna, J.A. (2005). RNA-mediated interaction between the peptide-binding and GTPase domains of the signal recognition particle. Nat. Struct. Mol. Biol. **12:** 1116–1122.

Stengel, K.F., Holdermann, I., Wild, K., and Sinning, I. (2007). The structure of the chloroplast signal recognition particle (SRP) receptor reveals mechanistic details of SRP GTPase activation and a conserved membrane targeting site. FEBS Lett. **581:** 5671–5676.

Sugiura, C., Kobayashi, Y., Aoki, S., Sugita, C., and Sugita, M. (2003). Complete chloroplast DNA sequence of the moss *Physcomitrella patens*: evidence for the loss and relocation of rpoA from the chloroplast to the nucleus. Nucleic Acids Res. **31:** 5324–5331.

Tzvetkova-Chevolleau, T., et al. (2007). Canonical signal recognition particle components can be bypassed for posttranslational protein targeting in chloroplasts. Plant Cell **19:** 1635–1648.

Valent, Q.A., Scotti, P.A., High, S., de Gier, J.W., von Heijne, G., Lentzen, G., Wintermeyer, W., Oudega, B., and Luirink, J. (1998). The *Escherichia coli* SRP and SecB targeting pathways converge at the translocon. EMBO J. **17:** 2504–2512.

Waldminghaus, T., Gaubig, L.C., Klinkert, B., and Narberhaus, F. (2009). The *Escherichia coli* ibpA thermometer is comprised of stable and unstable structural elements. RNA Biol. **6:** 455–463.

Zhang, X., Kung, S., and Shan, S.O. (2008). Demonstration of a multistep mechanism for assembly of the SRP x SRP receptor complex: implications for the catalytic role of SRP RNA. J. Mol. Biol. **381:** 581–593.

Zhang, X., Schaffitzel, C., Ban, N., and Shan, S.O. (2009). Multiple conformational switches in a GTPase complex control co-translational protein targeting. Proc. Natl. Acad. Sci. USA **106:** 1754–1759.

Zopf, D., Bernstein, H.D., Johnson, A.E., and Walter, P. (1990). The methionine-rich domain of the 54 kd protein subunit of the signal recognition particle contains an RNA binding site and can be crosslinked to a signal sequence. EMBO J. **9:** 4511–4517.

Zuker, M. (2003). Mfold web server for nucleic acid folding and hybridization prediction. Nucleic Acids Res. **31:** 3406–3415.